# Clouds, Hazes, and the Stratospheric Methane Abundance In Neptune

Kevin H. Baines

Jet Propulsion Laboratory, California
Institute of Technology
M.S. 169-237
4800 Oak Grove Drive
Pasadena, California 91109
818-354-0481

and

Heidi B. Hammel

Massachussetts Institute of Technology
54-416
Department of Earth, Atmospheric, and
Planetary Sciences
Cambridge, Massachusetts 02139
617-253-7568

Submitted to Icarus, June 25, 1993

Manuscript Pages: 46
Number of Figures: 19
Number of Tables: 4

Key Words: Neptune, Atmosphere
Abundances, Atmospheres
Atmospheres, Composition
Atmospheres, Structure
Clouds

Proposed Running Head:

Aerosols and Stratospheric Methane in Neptune

Send Editorial Correspondence and Proofs to:

Dr. Kevin H. Baines

M/S 169-237

Jet Propulsion Laboratory

4800 Oak Grove Drive

Pasadena, Ca 91109

## ABSTRACT

Analysis of high-spatial resolution ( ~ 0.8 arcsec) methane band and continuum imagery of Neptune's relatively homogeneous Equatorial Region yields significant constraints on (1) the stratospheric gaseous methane mixing ratio ($f_{CH_4,S}$), (2) the column abundances and optical properties of stratospheric and tropospheric hydrocarbon hazes, and (3) the wavelength-dependent single-scattering albedo of the 3-bar opaque cloud. From the center-to-limb behavior of 7270-Å and 8900-Å $CH_4$ bands, the stratospheric methane mixing ratio is limited to $f_{CH_4,S} < 1.7\ 10^{-3}$, with a nominal value $f_{CH_4,S} = 3.5\ 10^{-4}$, one to two orders of magnitude less than pre-Voyager estimates, but in agreement with a number of recent ultraviolet and thermal infrared measurements, and largely in agreement with the tropopause mixing ratio implied by Voyager temperature measurements. Upper limits to the stratospheric haze mass column abundance and 6190-Å and 8900-Å haze opacities are 0.61 μg $cm^{-2}$ and 0.075 and 0.042, respectively, with nominal values of 0.195 μg $cm^{-2}$ and 0.0245 and 0.0137 for the 0.2-μm radius particles preferred by the recent Voyager PPS analysis of Pryor *et al.* (1992, *Icarus* **99**, 302-316). The tropospheric $CH_4$ haze opacities are comparable to that found in the stratosphere, i.e, upper limits of 0.104 and 0.065 at 6190 Å and 8900 Å, respectively, with nominal values of 0.085 and 0.058. This indicates a column abundance less than 11.0 μg $cm^{-2}$, corresponding to the methane gas content within a well-mixed, 3%-methane tropospheric layer only 0.1 cm thick. Constraints on the single-scattering albedos of these hazes include: (1) for the stratospheric component, 6190-Å and 8900-Å imaginary indices of refraction less than 0.047 and 0.099, respectively, with

0.000 (conservative scattering) being the nominal value at both wavelengths, and (2) $CH_4$ haze single-scattering albedos greater than 0.85 and 0.50 at these same two wavelengths, with conservative scattering again being the preferred value. However, conservative scattering is ruled out for the opaque cloud near 3 bars marking the bottom of the visible atmosphere. Specifically, we find cloud single-scattering albedos of 0.915 ± 0.006 at 6340 Å, 0.775 ± 0.012 at 7490 Å, and 0.803 ± 0.010 at 8260 Å. Global models utilizing a complete global spectrum confirm the red-absorbing character of the 3-bar cloud. The global-mean model has ~ 7.7 times greater stratospheric aerosol content than the Equatorial Region. Finally, re-analysis of the Voyager PPS 7500-Å phase angle data utilizing the $f_{CH_4,S}$ and $P_H$ value derived here confirms the Pryor *et al.* (1992) result of a tropospheric $CH_4$ haze opacity of a few tenths in the 22-30°S latitude region, several times that of the Equatorial Region or of the globe. The factor-of-ten reduction in $f_{CH_4,S}$ below that assumed by Pryor *et al.* implies decreased gas absorption and consequently a decrease in the forward scattering component of tropospheric aerosols.

## I. INTRODUCTION

Our present understanding of the optical/microphysical properties and vertical distribution of aerosols in Neptune's atmosphere is somewhat precarious. Due to the substantial spatial and temporal variability of Neptune's meteorologically-active atmosphere, as revealed over the years in spectra and imagery acquired from the ground (*e.g.*, Joyce *et al.* 1977; Brown *et al.*, 1981; Hammel and Buie, 1987; Hammel, 1989; Hammel *et al.*, 1992)

and from space (*e.g.*, B. A. Smith *et al.*, 1989), results derived from full-disk observations spanning several years (*e.g.*, Baines and Smith, 1990) are, to an uncertain degree, imprecise. More importantly, the large (several orders of magnitude) decrease in estimates of the stratospheric methane mixing ratio ($f_{CH_4,S}$) reported over the last several years by both ground-based and spacecraft-borne instruments implies a significant revision in the aerosol structure derived from $f_{CH_4,S}$-sensitive methane band observations. In particular, the substantial decrease in $f_{CH_4,S}$ from 1-3% in the late 1980's (Orton *et al.*, 1987) to current estimates of $10^{-5}$ - $10^{-3}$ (Orton *et al.*, 1992; Yelle *et al.*, 1993) warrants a re-analysis of the stratospheric and tropospheric aerosol opacitites and column mass abundances previously estimated, for example, by Hammel *et al.* (1989) and Baines and Smith (1990) from visible and near-infrared methane band imagery and spectra.

In this paper, we utilize spatially resolved, high signal-to-noise center-to-limb observations of the especially homogeneous and quiescent Equatorial Region (ER) of Neptune to reliably determine aerosol properties within a specific, structurally-uniform region of the planet. The data, consisting of imagery acquired 21 May 1986 by Hammel *et al.* (1989) in three continuum wavelengths and three neighboring methane bands of varying strengths, allows the stratospheric methane mixing ratio to be derived as well, affording a self-consistent model of aerosol and gas abundances. In addition, we investigate globally-averaged models, based on the global visible-near-infrared spectrum of Neff *et al.* (1984, 1985) and the IUE spectrum previously assessed by Baines and Smith (1990), using the ER parameters as a starting point. Pseudo-continuum wavelengths observed in the Neff

*et al.* data are used to assess optical properties at the bottom of the visible atmosphere at wavelengths unobserved by Hammel *et al.* (1989). Finally, we compare the expected intensities predicted by the Equatorial Region and global models to that observed over a variety of phase angles for a narrow latitude band from 22° to 30° S by Voyager, to assess the viability of our models to this uniquely-observed region.

FIGURE 1

The parameters to be determined for the Equatorial Region are depicted in Figure 1. These include the stratospheric methane mixing ratio; the column abundance, opacity, and single-scattering albedo of stratospheric aerosols; the column abundance, opacity, and single-scattering albedo of the tropospheric methane haze; and the single-scattering albedo of the 3-bar cloud at the bottom of the visible atmosphere. For the global model, the stratospheric haze column abundance and single-scattering albedo of the bottom cloud are constrained using wavelengths unobserved in the Equatorial Region.

## II. PARAMETERIZATION

The analysis procedure largely follows that of Baines and Smith (1990), utilizing essentially the same haze and cloud morphology (*c.f.*, Figure 1) and radiative transfer codes. Salient variations between the previous analysis and the present work include: (1) the use of relevant parameters determined by Voyager, including phase function parameters (Pryor *et al.,* 1992) and the thermal profile (Tyler *et al.*, 1989), (2) the use of low-temperature

methane absorption coefficients (Karkoschka and Tomasko, 1992), and (3) improvements in the radiative transfer code. In particular, this code was modified to allow the methane mixing ratio in the non-saturated, warm upper stratosphere to be different than that assumed for the warm lower troposphere (in colder regions, the mixing ratio follows that predicted by the Clausius-Clapeyron relation). Thus, in this investigation, $f_{CH_4,S}$ is a free parameter which is allowed to vary, contrary to previous studies (*e.g.*, Hammel *et al.*, 1989; Baines and Smith, 1990; Pryor *et al.*, 1992).

Our morphology includes a stratospheric haze region, with the principal components being ethane, acetylene, and diacetylene. As theoretically determined by Romani *et al.* (1989), ethane comprises ~ 82% of the aerosol burden by volume, with acetylene making up the bulk of the remainder (~ 17%). As in Baines and Smith (1990), these aerosols are treated as Mie scatterers utilizing a log-normal distribution of width $\sigma = 1.35$ for number densities. As indicated in Figure 1, the vertically-averaged imaginary index of refraction, the mean particle size, and total column number density are left as free parameters to be determined by the analysis.

In the troposphere, a methane haze layer with a base near 1.54 bar is expected assuming the Baines and Smith (1990) deep-troposphere methane mixing ratio, $f_{CH_4,t}$ of 0.03. We note that this value was derived from measurements of the shapes and equivalent widths of weak individual lines of hydrogen and methane which are especially sensitive to atmospheric pressure and $CH_4$ content within the troposphere, and is not very sensitive to the properties

of optically thin ($\tau \lesssim 1$) hazes in the stratosphere or upper troposphere under analysis here. Thus $f_{CH_4,t}$ is not a free parameter. On the other hand, the $CH_4$ hazetop pressure is a free parameter which is derived rather than assumed in our analysis (again, unlike previous investigations). Additionally, the opacity and single-scattering albedo are parameters to be determined at several wavelengths. These are evaluated with two types of phase functions. First, we use the double Henyey-Greenstein phase function of Pryor *et al.* (1992), as developed from 0.75-μm Voyager PPS measurements of a 22° - 30°S latitude band observed over a range of phase angles. Specifically, parameter values are $g_1 = 0.900$, $g_2 = -0.11$, and $f_1 = 0.42$. Second, Mie scatterers are used assuming a radius of 2.5 μm as estimated by Conrath *et al.* (1991b) from IRIS data. This allows the derivation of methane haze opacities and column densities from visible-near-infrared data which may be directly comparable to the IRIS thermal-infrared results.

The bottom cloudtop is assumed to reside at 3.3 bars, again following the Baines and Smith (1990) molecular line analysis. This cloud is assumed to be optically thick ($\tau >> 10$), and is assumed characterized by the Pryor *et al.* (1992) phase function. The single-scattering albedo of this cloud over wavelength is to be constrained by the analysis, as indicated in Figure 1.

The helium molar fraction is assumed to be 0.15 (Conrath *et al.*, 1991b). This analysis is not sensitive to helium; thus the range of helium mixing ratios recently suggested by Conrath *et al.* (1993) does not impact the results derived here. Equilibrium hydrogen is

adopted, as determined by Baines and Smith (1990); again the analysis presented here is largely insensitive (except at 8260 Å; *c.f.* Section III.E) to the *ortho/para* distribution.

The method used to determine the various unknowns circled in Figure 1 involves constraining both the center-of-disk intensities and center-to-limb (CTL) behaviors of the six methane band and continuum filter images of Hammel *et al.* (1989). First, each of the three methane band images - one each at 6190, 7270, and 8900 Å - is investigated against five parameters: the opacity ($\tau_H(\lambda)$) and hazetop pressure of the tropospheric methane haze ($P_H$), the stratospheric methane mixing ratio ($f_{CH_4,S}$), and the stratospheric aerosol mean radius ($<r_s>$) and aerosol column abundances ($m_s$ and $N_s$, and $m_H$ and $N_H$, for mass and column densities, respectively, of the stratospheric aerosol and tropospheric $CH_4$ haze). A substantial range of values is explored for each of the first four parameters, spanning plausible ranges resulting from previous work (*e.g.*, Baines and Smith, 1990; Pryor *et al.*, 1992) as well as physical considerations. For each combination of values of these four parameters, and for each of the three methane band wavelengths, the value of the fifth parameter, the column abundance of the stratospheric haze, is determined which fits the center-of-disk intensity for that wavelength. The center-of-limb behavior, as measured by the standard deviation of the model/data CTL profile, is used to evaluate the goodness of fit of each model solution which matches the center-of-disk measurements. The values of these standard deviations are used to determine the best-fit values of the various parameters, P, and their own standard deviations, $\sigma_{rms}$ (P), the latter via the radius of curvature formula (*e.g.*, Orton and Ingersoll, 1976; Baines and Bergstralh, 1986):

$$\sigma_{rms}(P) = [(m-n)/r\ \partial^2 r/\partial^2 P]^{-1/2}. \qquad (1)$$

Here r is the standard deviation, or residual, of the model fit to the observations and m-n is the number of degrees of freedom, here conservatively assumed to be 1.

Additional constraints on parameter values include the physical boundary conditions that opacities can not be negative, that single-scattering albedos lie between 0.0 and 1.0 (inclusive), and that haze opacities monotonically decrease over wavelength from blue to red wavelengths. Finally, continuum bands are used to evaluate the imaginary index of refraction ($n_i$) of stratospheric hazes, and, for the troposphere, the single-scattering albedos of the methane haze and bottom cloud.

## III. RESULTS

### A. Constraints on Hydrocarbon Aerosol Opacities and Column Abundances

FIGURE 2

Figure 2 shows combinations of methane haze opacities and stratospheric haze number densities (here parameterized as $\rho_{C_2H_6}$, the number density of the ethane layer) which yield the center-of-disk I/F for each of the three methane bands, for set values of the stratospheric methane mixing ratio, stratospheric mean particle size, and methane hazetop

pressure. The relevant standard deviations, $\sigma_F$, between the modelled and observed center-to-limb profiles, here depicted in fractional units, are shown in Figure 3. Low values FIGURE of $\sigma_F$ for 6190 Å and 7270 Å correspond to relatively low values of $\rho_{C_2H_6}$. The minimum and curvature of the 6190-Å standard deviation curve yield the best-fit 6190-Å solution and standard deviation of $\rho_{C_2H_6}$ depicted as the circle and error bar in Figure 3. This solution constraint bar is also shown in Figure 2, but is truncated at the lowest $\rho_{C_2H_6}$ values due to the violation of the optical constraint that opacity not increase with wavelength (hereafter referred to as the "$\tau_{7270}/\tau_{8900}$ optical constraint"). Specifically, the opacity at 8900 Å exceeds that at 7270 by more than the amount that can be accounted for by uncertainties in I/F calibrations, - i.e. 0.013 I/F units, - for low values of $\rho_{C_2H_6}$ to the left of the vertical shaded lines shown in Figure 2. Thus we find that the stratospheric ethane number density is $\sim 5^{+6}_{-4}$ $cm^{-3}$, corresponding to a haze opacity of approximately 0.025 ± 0.02 for the three methane bands, as depicted in the various secondary axes near the bottom of Figure 2.

FIGURE 4

We conducted similar analyses over the full ranges of $f_{CH_4,S}$, $\langle r_s \rangle$, and $P_H$. As shown, for example, in Figure 4 (*c.f.*, alternate axes), we find that the best-fit solutions correspond to low stratospheric haze opacities near 0.025, regardless of the values chosen for the stratospheric particle size, stratospheric methane abundance, or tropospheric methane hazetop pressure. These figures show best-fit and standard deviations of $\rho_{C_2H_6}$ as a function of $P_H$, the hazetop pressure. The $\tau_{7270}/\tau_{8890}$ optical constraint is also shown, as well as the hazetop pressure constraint derived from a radius-of-curvature analysis of the 8900-Å CTL standard deviations (see discussion in Section III). Together, these constraints restrict

acceptable solutions of $\rho_{C_2H_6}$ and $P_H$ to relatively narrow ranges.

FIGURE 5

Figure 5 shows associated constraints on the tropospheric haze opacity, based on the restrictions shown in Figure 4 and the direct mapping relationship between $\rho_{C_2H_6}$ and $\tau_H$ shown in Figure 2. It is found that $\tau_H$ at 6190 Å typically lies in the range 0.05-0.10, regardless of the value of the stratospheric particle size, stratospheric methane abundance, or tropospheric methane hazetop pressure. A significant constraint on the maximum $CH_4$ haze opacity is placed by the "hazeless limit", beyond which the stratospheric haze opacity must be negative (meaning an unphysical, negatively attenuating, i.e., emitting, region) in order to match the center-of-disk reflectivity.

We find that our constraints on methane haze opacity are somewhat sensitive to the choice of phase function parameter values and methane absorption coefficients. We investigated the effect of using "end point" values of the range of phase function parameters reported by Pryor *et al.* (1992). Specifically, we used $g_2 = -0.201$ and $f_1 = 0.3933$ instead of the nominal $g_2 = -0.110$ and $f = 0.42$, thus doubling the backscattering component. We find that the derived opacities are typically 33% smaller at all three wavelengths (6190 Å, 7270 Å, and 8900 Å). We also find that using room-temperature coefficients of Giver (1978), instead of the low-temperature coefficients of Karkoschka and Tomasko (1992), increases the derived opacities at 7270 Å and 8890 Å by 10% and 20%, respectively. However, we find that 6190-Å opacities are significantly less than 7270 Å opacities in all of our solutions that utilize room-temperature coefficients, thus further mitigating against the

use of such coefficients for the analysis of Neptune's cold atmosphere.

We also have utilized Mie scattering particles for the methane haze. This allows estimates of particle size and mass and number column densities to be derived which can be compared to estimates derived at other wavelengths, such as reported by the Voyager IRIS experiment near 50 μm (Conrath *et al.* 1991b). The number and mass column densities may also be compared to that expected from dynamical and microphysical considerations of convective upwelling, sedimentation, and coagulation processes.

In this analysis, we determine the mass column densities ($m_H$; μg cm$^{-2}$) of the methane haze which fit the center-of-disk intensities at each of the three methane band wavelengths at 8900, 7270, and 6190 Å. The Mie scatterers are evaluated using the parameters of a standard model, depicted in Figures 2-5 as SM2, (specifically, $f_{CH_4,S}$ = 0.00035, $P_H$ = 0.34 bars, $\rho_{C_2H_6}$ = 5.25 cm$^{-3}$, $\langle r_s \rangle$ = 0.2 μm). As shown in Figure 6, over particle sizes from 0.1 to 4.0 μm, we find mass column densities of 7 ± 3 μg cm$^{-2}$, with the best agreement (as determined by the smallest variation in mass column density solutions satisfying each of the three wavelengths) for 2.5 μm, where $m_H$ = 7.81 ± 1.09 μg cm$^{-2}$ is derived. As discussed below in Section III.D, these results depend little on the choice of standard model since the opacity of the methane haze varies by less than 2% between them (*c.f.*, Table II.).

FIGURE 6

FIGURE 7

For Pryor phase function scatterers, the maximum methane haze opacity is summarized over the full range of plausible $f_{CH_4,S}$, $P_H$, and $\langle r_s \rangle$ in Figures 7 and 8. Once again, the

FIGURE 8

hazeless and $\tau_{7270}/\tau_{8890}$ opacity limits place constraints on the maximum opacity, restricting $\tau_H(6190) < 0.10$ (Figure 7) and $\tau_H(8900) < 0.07$ (Figure 8). Constraints on the maximum $f_{CH_4,S}$ allowed are also depicted in these figures, as determined by the condition that $\tau_H(8900) > 0.13$ (to prevent $\tau_H(7270)$ from being negative). $f_{CH_4,S} < 4\ 10^{-3}$ is indicated. Tighter constraints can be placed on $f_{CH_4,S}$ from the standard deviation between the observed and modelled center-to-limb profiles of the strongest methane bands, as we now discuss.

B. Constraints on Stratospheric Methane Mixing Ratio. FIGURE 9

FIGURE 10

As shown in Figures 9 and 10, the strong 8900-Å and 7270-Å methane bands are sensitive to the stratospheric methane mixing ratio. The limb darkening behavior of the 8900-Å band is particularly diagnostic, as illustrated in Figure 9. The standard deviations of such observed/modelled CTL profiles are utilized in the radius-of-curvature formula (Eq., 1) to derive constraints on $f_{CH_4,S}$, as depicted in Figure 10. Evaluating over hazetop pressure and particle size, constraints on $f_{CH_4,S}$ over the full range of parameters in our analysis are shown in Figure 11. Additional constraints on $f_{CH_4,S}$ are placed by (1) the physical limitation that opacities can not be negative, and (2) that opacities do not increase with wavelength. Large methane mixing ratios (> 0.002) require unphysical 7270-Å opacities < 0, and thus are ruled out. As shown in Figure 11, this analysis indicates $f_{CH_4,S} < 0.0017$, with a preferred range $2\ 10^{-5}$ - $10^{-3}$. Simultaneously, the analysis indicates a

FIGURE 11

tropospheric methane hazetop pressure $0.1 < P_H < 0.65$ bars, with a preferred range $0.1 < P_H < 0.52$ bars.

The models utilized to produce Figure 11 incorporate the methane haze opacities and stratospheric number densities which best-fit the 6190-Å data. We find that our $f_{CH_4,S}$ results are independent of the choice of number densities ($\rho_{C_2H_6}$) and methane haze opacities ($\tau_H$) which fit the 8900-Å center-of-disk data (various combinations of which are shown, for example, in Figure 2). This is due to the relative invariance of the 8900-Å standard deviation over these ($\rho_{C_2H_6}$,$\tau_H$) combinations, as shown, for example, in Figure 3. Thus, the choice of any ($\rho_{C_2H_6}$,$\tau_H$) combination leads to essentially the same constraints shown in Figure 11.

We find as well that our $f_{CH_4,S}$ results are insensitive to the range of tropospheric phase functions allowed by the Pryor *et al.* (1992) analysis. However, constraints on $f_{CH_4,S}$ depend somewhat on $<r_s>$, the stratospheric particle radius. For example, the maximum plausible $f_{CH_4,S}$ increases to $3\ 10^{-3}$ for $<r_s> = 0.3$ μm from $1.7\ 10^{-3}$ for 0.2 μm. The 0.2-μm curves shown in Figure 11 are accurate to within 20% for particle sizes between 0.15 and 0.20 μm, i.e., the range derived by Pryor *et al.* (1992) from Voyager UV measurements. Their preferred value of 0.2 is what we adopt here for our nominal models.

C. Constraints on Single Scattering Albedos

The above analysis places relatively tight constraints on the stratospheric and tropospheric hydrocarbon aerosol burden, as well as on the stratospheric methane mixing ratio, as a function of tropospheric hazetop pressure. We find that the interrelationship between these parameters places tight constraints on the range of plausible deep-cloud single-scattering albedos determined from continuum images at 6340 Å, 7490 Å, and 8260 Å. For example, setting $<r_s>$ = 0.2 μm, $f_{CH_4,S}$ = 0.0035, and $P_H$ = 0.34 bars (that is, the Standard Model 2, or SM2, values shown in Figures 2-5), we find that the single-scattering albedo of the bottom cloud, $\tilde{\omega}_{cld}$, is constrained to 0.9149 ± 0.0002, 0.7753 ± 0.0005, and 0.8025 ± 0.0024 at 6340 Å, 7490 Å, and 8260 Å, respectively, over the full range of valid $\rho_{C_2H_6}$ (i.e, the shaded portion of the horizontal solution bar around SM2 in Figure 4-b). Fixing $\rho_{C_2H_6}$ instead and letting $P_H$ vary over plausible limits (*e.g.*, fixing $\rho_{C_2H_6}$ at 5.25 $cm^{-3}$, the SM2 value, and letting $P_H$ vary between the limits of 0.24 bars and 0.41 bars, *c.f.*, Figure 4-b), we find that $\tilde{\omega}_{cld}$ = 0.9149 ± 0.0003, 0.7753 ± 0.0013, and 0.8025 ± 0.0037. We find small variations as well when different standard models (such as SM1 and SM3 shown in Figures 4, 5, and 11) are adopted. In particular, we find variations of 0.0001, 0.0006, and 0.0003 over the nominal numbers quoted above respectively for the three wavelengths. All of these variations are much smaller than that associated with the 3% absolute calibration uncertainty of the observed I/F. Specifically, we determine for SM2 single scattering albedos of $\tilde{\omega}_{cld}$ = 0.915 ± 0.006, 0.775 ± 0.012, and 0.803 ± 0.010 at 6340 Å, 7490 Å, and 8260 Å, respectively, where the uncertainties are due to absolute calibration uncertainties. As shown near the bottom of the right hand column of Table I, over all plausible combinations of $f_{CH_4,S}$, $<r_s>$, and $P_H$ (*c.f.* Figure 11, for example), we find that single scattering albedos lie

TABLE I

in the range 0.90-0.93, 0.75-0.80, and 0.78-0.82 for these three wavelengths.

Tight constraints are placed on the imaginary index of refraction, $n_i$, of the stratospheric haze by the limb-darkening observed in the strong 8900 Å $CH_4$ band as well as in the continuum bands. As $n_i$ is increased from 0.0, the total haze opacity of stratospheric and tropospheric hydrocarbon hazes increases significantly in order to match the I/F at the center-of-disk. This in turn leads to enhanced limb darkening, producing dramatic departures from good fits to the observed CTL profiles. In the strong 8900-Å methane band, we find $n_i < 0.099$. Analysis of the center-to-limb behavior at continuum wavelengths yields $n_i$ less than 0.047, 0.126, and 0.149 at 6340 Å, 7490 Å, and 8260 Å, respectively, with $n_i = 0.0$ yielding the minimum standard deviation at all wavelengths.

Constraints are not as tight for the methane haze. At 8900 Å, we find that decreasing $\tilde{\omega}_H$ leads to increased stratospheric and/or tropospheric haze abundances which again produces excessive limb darkening. Specifically, we find the center-to-limb profile to be unsatisfactorily matched for $\tilde{\omega}_H < 0.5$ at 8900 Å. Analysis of the continuum wavelengths indicates that $\tilde{\omega}_H$ is greater than 0.85, 0.65, and 0.60 at 6340 Å, 7490Å, and 8260 Å, respectively. We note that the single-scattering albedo limits quoted here for both the tropospheric and stratospheric hazes are the minima allowed based on an analysis wherein one haze is varied while the other is assumed conservatively scattering. If both hazes are allowed to vary simultaneously, then the minima increase.

Constraints on the methane haze imaginary index of refraction assuming Mie scattering particles are somewhat tighter. From the 3% calibration uncertainty, we find $n_i$ to be less than 0.0011 at 6340 Å and 7490 Å, and less than 0.00017 at 8260 Å, corresponding to minimum albedos of 0.940, 0.948, and 0.993 at these three wavelengths. As in the stratosphere, the minimum standard deviation between models and observations occurs for $n_i = 0.0$ at all wavelengths.

D. Summary of Equatorial Region Results

FIGURE 12

Table I summarizes results for the Equatorial Region. This table and Figure 12 lists values and uncertainties for the baseline model SM2, a model which nominally fits the 6190-Å center-to-limb profile and is in the midrange of nominal ($f_{CH_4,S}$, $P_H$) solutions as depicted in Figures 4, 5, and 11. This model incorporates $\langle r_e \rangle = 0.2$ μm, $f_{CH_4,S} = 0.00035$, $P_H = 0.34$ bars, $\rho_{C_2H_6} = 5.245$ cm$^{-3}$, and $\tau_H$ (6190 Å) = 0.085. The fit of this model to the observations is depicted in the center-to-limb profiles shown in Figure 13. Other standard models SM1, and SM3 depicted in Figure 11 are for different combinations of $f_{CH_4,S}$ and $P_H$ which lie within the nominal unshaded region of the figure. We find that the values of $\rho_{C_2H_6}$ and $\tau_H$(6190Å) as well as the single-scattering albedos of the various hazes and clouds for these models vary for the most part by less than 10% from the SM2 values, as shown in Table II.

FIGURE 13

TABLE II

FIGURE 14

Figure 14 shows the opacities of the various hydrocarbon aerosols in the stratosphere and troposphere. Again, the figure depicts SM2 values which vary little for all plausible models. All layers show opacities less than 0.1 throughout the visible/near-infrared. The stratospheric aerosol opacity, comprising the sum of the $C_2H_6$, $C_2H_2$, and $C_4H_2$ opacities, is less than 0.01 at wavelengths greater than 9500 Å. Both the Mie-scattering solution and the double Henyey-Greenstein phase function solution indicate opacities less than 0.1 for the tropospheric methane haze throughout the analyzed wavelength range. Over all plausible models, upper limits of 0.07 and 0.12 are found longward of 7270 Å for the double Henyey-Greenstein and Mie scattering cases, respectively.

FIGURE 15

Figure 15 shows the single-scattering albedo for the bottom cloud compared to previous solutions of Baines and Smith (1990) and Pryor *et al.* (1992). Beyond the three continuum wavelength values discussed thus far in this paper, additional values are depicted which come from a re-analysis of the global broadband visible spectrum of Neff *et al.* (1984,1985) and the global IUE spectrum of Baines and Smith (1990), as discussed in the next section.

## E. Global Model Constraints

The global spectral datasets previously analyzed by Baines and Smith (1990) were re-examined to (1) determine the efficacy of the Equatorial Region model for the mean globe; (2) determine constraints on the bottom cloud albedo at other wavelengths, here using the Karkoschka and Tomasko (1992) low-temperature coefficients as opposed to the

Giver (1978) room-temperature coefficients previously used by Baines and Smith (1990); and (3) determine the mean global imaginary index of refraction to use in the ultraviolet and blue-yellow. A comparison between the global UV determination and that determined by the Voyager PPS (Pryor *et al.* 1992) for a relatively narrow latitudinal band provides information on spatial and/or temporal variability of UV absorbers in the upper stratosphere. In the blue-yellow, the variability in $n_i$ required to match the 4% global variability observed by Lockwood and Thompson (1986) is useful in gauging the plausibility of the Baines and Smith (1990) hypothesis that solar-cycle induced uv-irradiation of stratospheric particles causes the observed blue-yellow variability.

At 8900 Å, the global geometric albedo (observed in 1981) is some 50% greater than predicted by the Equatorial Region (ER) center-to-limb curve (acquired in 1986). In addition to temporal variability on yearly and monthly scales (*c.f.* Lockwood *et al.*, 1991), spatial variability is indicated, as supported by the 8900-Å image itself (*c.f.*, Hammel *et al.*, 1989) which shows the ER to be substantially darker than the surrounding brighter temperate/polar regions, thus indicating that the global stratospheric haze content and associated particle scattering is significantly enhanced over that found in the ER. Supporting evidence for spatial variability in the stratosphere comes from the IUE spectrum (Baines and Smith, 1990), which was acquired in 1986 within two months of the ER data. Specifically, as shown in Figure 16, we find that only relatively large UV opacities, i.e, several times greater than derived here for the ER, yield reasonable $n_i$ to match the 2000 and 2600 Å global IUE data. FIGURE 16

FIGURE 17

To match the 8900-Å geometric albedo, we find that 7.7 times the ER stratospheric content is required, assuming the methane haze opacity is fixed at the ER value (*c.f.*, Figure 17). The derived stratospheric content is not insensitive to the assumed tropospheric content. Increasing the methane haze opacity by 50% reduces the stratospheric abundance somewhat to 6.5 times the ER value. However, an upper limit of twice the SM2 $CH_4$ haze opacity is placed by the intermediate methane bands, which would otherwise be modelled too bright, thus placing a lower limit of 5.3 times the ER value on the global stratospheric haze abundance.

The ultraviolet provides strong supporting evidence for an enhanced global stratospheric haze. At 2000 Å, the analysis is insensitive to the methane haze since strong Rayleigh scattering and stratospheric haze absorption allows only a few percent of the multiply-scattered solar photons to travel to the troposphere. We find, as indicated in Figure 16, that the nominal 2000-Å geometric albedo is matched for plausible $n_i < 0.1$ only when the haze content is at least 6.0 time greater than the ER value. For the model with 7.7 times the ER stratospheric content (hereafter referred to as the nominal global model), $n_i = 0.05$ to fit the nominal 2000 Å geometric albedo, with $n_i = 0.018$ fitting the 2000-Å minimum limit. At 2600 Å, $n_i = 0.018\ ^{+0.022}_{-0.016}$. This is in agreement with the 2650-Å Voyager PPS determination of $n_i = 0.03 \pm 0.01$, thus suggesting that the 22° - 30° S latitude band observed by Voyager in the ultraviolet is a microcosm of the globally-averaged stratosphere.

Fitting several pseudo-continuum wavelengths in the global spectrum, we find the bottom cloud single-scattering albedo decreases between 6030 and 6910 Å. Specifically, as plotted in Figure 15, we find, for the nominal global model $\tilde{\omega}_{cld}$ is 0.911 ± 0.010 at 6030 Å, 0.867 ± 0.012 at 6450 Å, 0.828 ± 0.014 at 6780 Å, and 0.812 ± 0.017 at 6910 Å, where the uncertainties reflect the 3% calibration uncertainty of the Neff *et al.* (1984, 1985) spectrum. In the near-infrared at 9390 Å, the derived single-scattering albedo of 0.829 ± 0.101 (*c.f.*, Figure 17) confirms the trend observed in the 8260-Å band Equatorial Region analysis that the single-scattering albedo increases beyond about 7500 Å.

Figure 17 shows the fit of our nominal global and Equatorial Region models to the geometric albedo beyond 7700 Å. As noted earlier, the global model, with its enhanced high-altitude aerosol scattering, is a superior fit to the spectrum in the strong 8900 Å $CH_4$ band. However, neither model fits the region around 8260 Å, specifically the $S_3(0)$ pressure-induced absorption feature which appears excessively deep in our models. As shown in Figure 18, the 8260-Å feature can be matched by increasing the methane haze opacity, thereby limiting the mean hydrogen absorption pathlength. However, the mean methane absorption pathlength is then reduced as well, producing excessively bright models within the intermediate methane bands. Non-equilibrium hydrogen distributions, such as that shown in Figure 18 wherein 86% of the hydrogen is distributed according to the normal distribution of states and 14% is distributed according to the equilibrium distribution (designated as $f_{eH_2}$ = 0.14; *c.f.* Baines and Bergstralh 1986), produces a much more satisfactory fit to the 8260-Å $H_2$ feature and the surrounding spectrum. However, this

FIGURE 18

violates the near-equilibrium hydrogen distribution constraint placed by the 4-0 S(0) and S(1) features (Baines and Smith, 1990). As was the case for Uranus (Baines and Bergstralh, 1986), we suspect that the discrepancy is due to uncertainties in the absorption coefficients for cold ($\sim$90K) methane within the shoulder of this particular band.

The nominal global model indicates that $n_i$ for the stratospheric haze is nominally 0.012 at 4720 Å and 0.0055 at 5510 Å, i.e., the blue and yellow wavelengths observed by Lockwood and Thompson (1986). We find that a 4% variation in I/F can be matched by variations of 0.022 and 0.011 in the blue and yellow, respectively. This result is 5-10 times the change in $n_i$ derived by Baines and Smith (1990), corresponding to the factor of ten decrease in 0.5-μm opacity from 0.34 (Baines and Smith, 1990) to 0.031 derived here (Figure 16).

F. 25°S Latitude/Global/Equatorial Region Comparison

We examined the 7500-Å PPS data of the 22-30°S latitude region to investigate the degree of agreement with our baseline Equatorial Region and global models. We find the fit to the SM2 baseline ER model to be unsatisfactory. Specifically, the modelled intensities at low phase angles are 30-40% lower than observed, indicating an enhancement in scattering aerosols. The nominal global model, with 7.7 times the stratospheric aerosol content of the ER baseline, produces a slightly better, but still unsatisfactory fit. We find

that increasing the methane haze opacity to 0.24-0.34 yields good fits to the 14-72° phase angle data, for both the Equatorial Region and global models, as shown by the circles in Figure 19. This is in agreement with the Pryor *et al.* (1992) analysis, confirming that the methane haze opacity and abundance may be significantly greater in this region then (1989) than in the Equatorial Region (1986) or the mean globe (1981-1986). For this modified global model (panel A), the fit is not very satisfactory at high phase angles, as the modelled I/F is some 50% greater than that observed at both 132 and 159 degrees phase angle. The modified Equatorial Region model does a better job, as the 7.7 times less optically thick stratospheric haze layer significantly reduces the forward scattering of light through the atmosphere. Indeed, this model achieves too little forward scattering, producing an underestimation of the observed I/F. A doubling of the stratospheric aerosol content found in the Equatorial Region produces satisfactory fits to the high phase angle 7500-Å data. However, this then is 3.5 times less than the aerosol burden derived for this region from the UV by Pryor *et al.* (1992) and the global burden derived here. To summarize, our analysis of 7500-Å Voyager PPS data indicates that the 22-30° South latitude region has a stratospheric aerosol burden between that found in the Equatorial Region and the global average, and has a methane haze which is significantly (approximately four times) that found in either the Equatorial Region or the global average.

# IV. DISCUSSION

## A. Stratospheric Methane

Our determination that the stratospheric methane mixing ratio lies between 2 $10^{-5}$ and 1.7 $10^{-3}$, with a nominal range 2 $10^{-5}$ - $10^{-3}$, is in agreement with a number of recent investigations. In particular, as illustrated in Figure 11, our nominal range compares favorably with both Voyager UVS (the entire range of Bishop *et al.*, 1992; as well as the lower limit of Yelle *et al.*, 1993) and ground-based thermal-IR determinations (Orton *et al.*, 1992). The lower portion of our nominal range (i.e, < 5 $10^{-4}$) is consistent as well with the $CH_4$ mixing ratio expected above the relatively warm coldtrap tropopause temperatures reported by Voyager IRIS (Conrath *et al.*, 1991a). Thus, consistent with the Bishop *et al.* (1992) analysis, we find that convection may not be required to supply methane to the troposphere, as had been previously postulated (*e.g.*, Hunten *et al.*, 1974; Appleby, 1986) to explain why the best pre-Voyager estimate of $f_{CH_4,S}$ (*e.g.*, Orton *et al.*, 1987) of ~ 0.02 was several orders of magnitude greater than predicted by the pre-Voyager relatively cold tropopause temperature. However, we are consistent as well with Yelle *et al.'s* (1993) lower limit of $f_{CH_4,S} = 6.10^{-4}$, some 50% greater than the maximum tropopause value ($f_{CH_4,S}$ = 4 $10^{-4}$) allowed by the warmest temperature (57 K) measured by Voyager, indicating that stratospheric $CH_4$ oversaturation and concomitant strong vertical transport of $CH_4$ - laden tropospheric gas may indeed occur. Unfortunately, then, our analysis is unable to resolve the discrepancy in $f_{CH_4,S}$ between the parallel UVS analyses of Bishop *et al.* (1992) and

Yelle *et al.* (1993), or to settle conclusively whether or not the stratosphere is oversaturated in methane.

B. Aerosol Structure Comparison

TABLE III

TABLE IV

We show in Tables III and IV a comparison of our stratospheric and tropospheric results with the findings of previous investigators, including Hammel *et al.* (1989), Baines and Smith (1990), and Pryor *et al.* (1992). Major differences in the assumed stratospheric methane mixing ratio, hazetop level, and phase functions, as well as differences in the regions studied, have led to a variety of values for various parameters. Due to the combination of a number of innovations introduced in this investigation (particularly the use of a range of plausible stratospheric methane abundances and self-consistent tropospheric $CH_4$ hazetop levels, the use of empirically-determined phase functions from Voyager, and the use of low-temperature methane absorption coefficients), we assert that the results of this study are a significant improvement over previous investigations.

All recent studies using UV to near-infrared radiation have thus far concluded that the methane haze has an opacity near or significantly less than unity (*c.f.*, Table III). In particular, our equatorial and global column mass abundance of 7.81 ± 1.1 $\mu g\ cm^{-2}$ yields a visible opacity of ~ 0.1. We also find, in agreement with Pryor *et al.* (1992), an opacity of several tenths in the 22-30° S region. However, these results are in disagreement with the Voyager IRIS determination of unity opacity near 50 μm, which strongly imply an

opacity two orders of magnitude larger in the visible (Conrath *et al.*, 1991b). This discrepancy may be resolved by recent modifications to the polar radius derived by Limaye and Sromovsky (1992), which may alter the radio occultation thermal profile by the 1K necessary to obviate the need for an optically-thick absorbing haze (Conrath, personal communication).

We note that our global stratospheric aerosol mass and column number densities are in remarkable agreement with that derived in the ultraviolet by Pryor *et al.* (1992), given the differences in the regions under analysis and techniques used (i.e., 22-30° S for Voyager high-phase angle UV photometry vs full-disk UV and methane-band absolute photometry). This implies that the 22-30° S region is a microcosm of the mean atmosphere while the ER is relatively depleted in aerosols. However, our finding of an aerosol-depleted ER is somewhat in disagreement with PPS scan imagery of the ER (Lane *et al.*, 1989; Pryor and Hord, 1991), which suggests that the stratospheric UV-absorbing haze is more abundant in the Equatorial Region than elsewhere. This discrepancy may be due to temporal variability - the groundbased data having been acquired in May, 1986 vs the Voyager data of August 1989. Quantitative analysis of such variability awaits detailed analysis of the Voyager PPS ER data.

Our picture of the 22-30° S region being a microcosm of the global stratosphere appears to break down at 7500-Å, where high phase angle data favors a depleted stratosphere close to that derived here for the ER. We note that our analysis used the nominal $f_{CH_4,S}$ derived

herein, i.e, 0.00035, an order of magnitude less than the 0.0035 value assumed by Pryor *et al.* (1992), and a tropospheric cloudtop situated at less than half the Pryor *et al.* pressure. We suggest that the resulting reduced atmospheric gas absorption implies a corresponding reduction in the forward scattering component of tropospheric aerosols. A re-evaluation of the tropospheric 7500-Å phase functions is warranted, utilizing the stratospheric methane mixing ratio and atmospheric aerosol structure derived here, in order to discover whether a significant reduction in forward scattering can resolve the UV/near-ir discrepancy in the stratospheric aerosol abundance.

C. Dynamical Implications

Our methane haze column mass abundance of ~ 7.81 $\mu g\ cm^{-2}$ corresponds to the amount of methane vapor in a 3% methane mixture of atmospheric gases near the 1.5 bar condensation level only 0.07 cm thick. Thus only a tiny fraction of the methane available to form aerosol particles is actually observed in the condensed state at any one time, consistent with theoretical considerations of particle growth and sedimentation (e.g, Carlson *et al.*, 1988).

As in Baines and Smith (1990), the stratospheric aerosol production rate may be estimated from the sedimentation rate and mass column density of the stratospheric haze, assuming steady state conditions. Specifically, we find that the 0.2-μm particles specified

here fall at 3.9 mbar/year (compared to 10.2 mbar/year for the 0.52-μm particles of Baines and Smith). The time for the major ethane haze layer to fall through itself is 10 mbar/(3.9 mbar/year) or 2.6 years. The mass of the ethane haze is ~ 0.82*1.5 μg $cm^2$ = 1.23 μg $cm^{-2}$, implying a haze loss rate of 0.48 μg $yr^{-1}$ or 1.5 $10^{-14}$ g $cm^{-2}$ $s^{-1}$, a factor of 1.9 - 41 less than the Baines and Smith (1990) estimate of 2.8 $10^{-14}$ - 6.2 $10^{-13}$ g $cm^{-2}$ $s^{-1}$. This is 50% greater than the theoretical methane destruction rate of $10^{-14}$ g $cm^{-2}$ $s^{-1}$ estimated by Romani *et al.* (1993), well within the error bar of our 8900-Å and IUE measurement uncertainty. As for the mass and column densities, we note that our global-mean value of 1.5 μg $cm^{-2}$ agrees reasonably well with the theoretical value of 4.7 μg $cm^{-2}$ calculated by Romani *et al.* (1993). The factor-of-three agreement is within the uncertainties which, beyond the observational uncertainties noted above, include for theoretical modelling (1) simplifying assumptions about vertical transport mechanisms, including the neglect of coagulation and coalescence, and (2) the uncertainty of various important hydrocarbon reaction rates and photolysis pathways (Romani, private communication).

The loss of stratospheric carbon due to the precipitation of hydrocarbon ice particulates implies that carbon is being resupplied to the stratosphere. As indicated in Figure 11, the maximum observed tropopause temperatures of ~ 57 K (Conrath *et al.* 1991a) indicate that upward diffusion of methane from the tropopause could maintain a stratospheric methane mixing ratio of ~ 5 $10^{-4}$. This methane abundance is below observed upper limits, as shown in Figure 11 (lower scales and SM1, for example). Thus, diffusion may be augmented by convection, as first suggested by Hunten (1974), conveying tropospheric material in the form

of methane ice crystals upward through three scale heights from the condensation level near 1.5 bars to the sublimation level near 60 mbars.

An upper estimate of the resupply rate indicates that the necessary convection need occupy only a tiny fraction of the Neptune's surface area. Based on a methane gas density of ~0.01 g $cm^{-2}$ per meter at the 3%-methane mixing ratio condensation level, we estimate that a single two-kilometer diameter storm, upwelling at an areal-mean velocity of 1 m $s^{-1}$ at the sublimation level and entraining 1% of the tropospheric methane vapor content, can deliver to the stratosphere the two metric tons per second of methane required to balance our nominal 1.9 $10^{-14}$ g $cm^{-2}$ $s^{-1}$ hydrocarbon precipitation rate. Thus only 2 $10^{-10}$ of the surface is required to be convective on the average. Such a storm would extend from the tropospheric $CH_4$ condensation level near 1.5 bars to the $CH_4$ sublimation level near 60 mbars, a distance of some 60 km. The energetics required to initiate and sustain such a storm seem problematical, although several mechanisms have been proposed (*e.g.*, Lunine and Hunten, 1989; Stoker and Toon, 1989).

The factor-of-eight depletion of stratospheric aerosols determined for the ER in 1986 relative to the global mean, as well as the Voyager PPS implication of an enhancement in the ER stratospheric aerosol burden in 1989, implies that both regional and temporal variability in aerosol heating is significant. Based on the Baines and Smith (1990) estimate that 6-14% of the incident solar flux in the visible is deposited, on average, in stratospheric aerosols above 20 mbar, we note that the ER aerosol depletion implies that as little as 1-2%

of the incident sunlight may be deposited there at times. Presumably, this means that the tropospheric deposition of sunlight could vary as well (i.e, more sunlight would be deposited in tropospheric $CH_4$ gas and aerosols during periods of stratospheric aerosol thinning). Clearly, the implications of such a variability on stratospheric, and underlying tropospheric, dynamics and global circulation warrants further quantitative investigation.

## ACKNOWLEDGMENTS

The work described in this paper was carried out by the Jet Propulsion Laboratory, California, under contract with the National Aeronautics and Space Administration, with support from the Neptune Data Analysis Program and the Planetary Atmospheres Discipline, NASA Office of Space Sciences and Applications.

## REFERENCES


Appleby, J. F. 1986. Radiative-convective equilibrium models of Uranus and Neptune. *Icarus* **65**, 383-405.

Baines, K. H. and J. T. Bergstralh. 1986. The structure of the Uranian atmosphere: Constraints from the geometric albedo spectrum and $CH_4$ line profiles. *Icarus* **56**, 543-559.

Baines, K. H.and W. H. Smith. 1990. The atmospheric structure and dynamical properties of Neptune derived from ground-based and IUE spectrophotometry. *Icarus* **85**, 65-108.

Bishop, J., S. K. Atreya, P. N. Romani, B. R. Sandel, and F. Herbert. 1992. Voyager 2 UVS solar occultations at Neptune: Constraints on the abundance of methane in the stratosphere. *J. Geophys. Res.* **93**, 11681 - 11695.

Brown, R. H., D. P. Cruikshank, and A. T. Tokunaga. 1981. The rotation period of Neptune's upper atmosphere. *Icarus* **47**, 159-165.

Carlson, B. E., W. B. Rossow, and G. S. Orton. 1988. Cloud microphysics of the giant planets. *J. Atmos. Sci.* **45**, 2066-2081.

Conrath, B. J., F. M. Flasar, and P. J. Gierasch. 1991a. Thermal structure and dynamics of Neptune's atmosphere from Voyager measurements. *J. Geophys. Res. Suppl.* **96**, 18,931 - 18,939.

Conrath, B. J., D. Gautier, G. F. Lindal, R. E. Samuelson, and W. A. Shaffer. 1991b. The helium abundance of Neptune from Voyager measurements. *J. Geophys. Res.* **96**, 18907-18919.

Conrath, B. J., D. Gautier, T. C. Owen, and R. E. Samuelson. 1993. Constraints on $N_2$ in Neptune's atmosphere from Voyager measurements. *Icarus* **101**, 168-171.

Giver, L. P. 1978. Intensity measurements of the $CH_4$ bands in the region 4350 Å to 10600. Å. *J. Quant. Spectrosc. Radiat. Transfer* **19**, 311 - 322.

Hammel, H. B. 1989. Neptune cloud structure at visible wavelengths. *Science* **244**, 1165 - 1167.

Hammel, H. B., K. H. Baines, and J. T. Bergstralh. 1989. Vertical aerosol structure of Neptune: Constraints from center-to-limb profiles. *Icarus* **80**, 416-438.

Hammel, H. B. and M. W. Buie. 1987. An atmospheric rotation period of Neptune determined from methane-band imaging. *Icarus* **72**, 62-68.

Hammel, H. B., S. L. Lawson, J. Harrington, G. W. Lockwood, D. T. Thompson, and C. Swift. 1992. An atmospheric outburst on Neptune from 1986 through 1989. *Icarus* **99**, 363-367.

Hunten, D. M. 1974. Introduction and summary. In *The Atmosphere of Uranus* (D. M. Hunten, Ed.). Proceedings of a NASA Workshop held at ARC, pp. 1-7.

Joyce, R. R., C. B. Pilcher, D. P. Cruikshank, and D. Morrison. 1977. Evidence for weather on Neptune. *Astrophys. J.* **214**, 657-662.

Karkoschka, E., and M. G. Tomasko. 1992. Saturn's upper troposphere 1986 - 1989. *Icarus* **97**, 161 - 181.

Lane, A. L., R. A. West, C. W. Hord, R. M. Nelson, K. E. Simmons, W. R. Pryor, L. W. Esposito, L. J. Horn, B. D. Wallis, B. J. Buratti, T. G. Brophy, P. Yanamandra-Fisher, J. E. Colwell, D. A. Bliss, M. J. Mayo, and W. D. Smythe. 1989. Photometry from Voyager 2: Initial results from the Neptunian atmosphere, satellites, and rings. *Science* **246**, 1450 - 1454.

Limaye, S. S. and L. A. Sromovsky. 1992. Winds, bands, and pole position and figure of Neptune: Voyager results. *Bull. Amer. Astron. Soc.* **24**, 973.

Lockwood, G. W, and D. T. Thompson. 1986. Longterm brightness variations of Neptune and the solar cycle modulation of its albedo. *Science* **234**, 1543-1545.

Lockwood, G. W. and D. T. Thompson. 1991. Solar cycle relationship clouded by Neptune's sustained brightness maximum. *Neptune* **349**, 593-594.

Lunine, J. I. and D. M. Hunten. 1989. Abundance of condensable species at planetary cold traps: The role of moist convection. *Planet. Space Sci.* **37**, 151-161.

Neff, J. S., T. A. Ellis, J. Apt, and J. T. Bergstralh. 1985. Bolometric albedos of Titan, Uranus, and Neptune. *Icarus* **62**, 425-432.

Neff, J. S., D. C. Humm, J. T. Bergstralh, A. L. Cochran, W. D. Cochran, E. S. Barker, and R. G. Tull. 1984. Absolute spectrophotometry of Titan, Uranus, and Neptune: 3500-10500 A. *Icarus* **60**, 221-235.

Orton, G. S., D. K. Aitken, C. Smith, P. F. Roche, J. Caldwell, and R. Snyder. 1987. The spectra of Uranus and Neptune at 8-14 and 17-23 μm. *Icarus* **70**, 1-12.

Orton, G. S. and A. P. Ingersoll. 1976. Pioneer 10 and 11 ground-based infrared data on Jupiter: The thermal structure and He-$H_2$ ratio. In *Jupiter* (T. Gehrels, Ed), pp 206-215.

Orton, G. S., J. H. Lacy, J. M. Achtermann, P. Parmar, and W. E. Blass. 1992. Thermal spectroscopy of Neptune: The stratospheric temperature, hydrocarbon abundances, and isotopic ratios. *Icarus* **100**, 541-555.

Pryor, W. R. and C. W. Hord. 1991. A study of photopolarimeter system UV absorption data on Jupiter, Saturn, Uranus, and Neptune: Implications for auroral haze formation. *Icarus* **91**, 161-172.

Pryor, W. R., R. A. West, K. E. Simmons, and M. Delitsky. 1992. High-phase-angle observations of Neptune at 2650 Å and 7500 Å: Haze structure and particle properties. *Icarus* **99**, 302-316.

Romani, P. N. and S. K. Atreya. 1989. Stratospheric aerosols from $CH_4$ photochemistry on Neptune. *Geophys. Res. Lett.* **16**, 941-944.

Romani, P. N., J. Bishop, B. Bezard, and S. Atreya. 1993. Haze production from $CH_4$ photochemistry in the stratosphere of Neptune. *Icarus*, submitted.

Smith, B. A., L. A. Soderblom, D. Banfield, C. Barnet, A. T. Basilevsky, R. F. Beebe, K. Bollinger, J. M. Boyce, A. Brahic, G. A. Briggs, R. H. Brown, C. Chyba, S. A. Collins, T. Colvin, A. F. Cook II, D. Crisp, S. K. Croft, D. Cruikshank, J. N. Cuzzi, G. E. Danielson, M. E. Davies, E. De Jong, L. Dones, D. Dodfrey, J. Goguen, I.

Grenier, V. R. Haemmerle, H. Hammel, C. J. Hansen, C. P. Helfenstein, C. Howell, G. E. Hunt, A. P. Ingersoll, T. V. Johnson, J. Kargel, R. Kirk, D. I. Kuehn, S. Limaye, H. Masursky, A. McEwen, D. Morrison, T. Owen, W. Owen, J. B. Pollack, C. C. Porco, K. Rages, P. Rogers, D. Rudy, C. Sagan, J. Schwartz, E. M. Shoemaker, M. Showalter, B. Sicardy, D. Simonelli, J. Spencer, L. A. Sromovsky, C. Stoker, R. G. Strom, V. E. Suomi, S. P. Synott, R. J. Terrile, P. Thomas, W. R. Thompson, A. Verbiscer, and J. Veverka. 1989. Voyager 2 at Neptune: Imaging Science Results. *Science* **246**, 1422 - 1449.

Stoker, C. R. and O. B. Toon. 1989. Moist convection on Neptune. *Geophys. Res. Letters* **16**, 928-932.

Tyler, G. L., D. N. Sweetman, J. D. Anderson, S. E. Borutzki, J. K. Campbell, V. R. Eshleman, D. L. Gresh, E. M. Gurrola, D. P. Hinson, N. Kawashima, E. R. Kursinski, G. S. Levy, G. F. Lindal, J. R. Lyons, E. A. Marouf, P. A. Rosen, R. A. Simpson, G. E. Wood. 1989. Voyager radio science observations of Neptune and Triton. *Science* **246**, 1466-1473.

Yelle, R. V., F. Herbert, B. R. Sandel, R. J. Vervack, Jr. and T. M. Wentzel, 1993. The distribution of hydrocarbons in Neptune's upper atmosphere. *Icarus*, in press.

## FIGURE CAPTIONS

Figure 1. Basic atmospheric structure utilized in the analysis. Parameters to be determined are circled. For the stratosphere, these include: $f_{CH_4,S}$, the $CH_4$ mixing ratio above the stratospheric condensation level; $n_i$, the mean imagery index of particulates; $<r_s>$, the mean particulate radius; and $N_s$, $m_s$, and $\tau_s(\lambda)$, the vertically-integrated number and mass column densities and wavelength-dependent aerosol opacity. For the troposphere, parameters to be determined include: $<r_H>$, the mean particle radius for the $CH_4$ haze; $\tilde{\omega}_H(\lambda)$ and $\tau_H(\lambda)$, the wavelength-dependent single-scattering albedo and optical depth of this haze; $N_H$ and $m_H$, the haze column and mass number densities; and $\tilde{\omega}_{cld}(\lambda)$, the wavelength-dependent single-scattering albedo of the bottom cloud. Other parameters, such as tropospheric methane mixing ratio ($f_{CH_4,t}$), *ortho/para* hydrogen characteristics (equilibrium ratio, defined as $f_{eH_2} = 1.0$), and base of the visible atmosphere ($P_{cld} = 3.3$ bars) are adopted from Baines and Smith (1990). Stratospheric condensation levels of various hydrocarbons, and relative weighting of stratospheric column number densities, are from Romani *et al.* (1989, 1993). Tropospheric phase function parameters are from Pryor *et al.* (1992). Thermal structure is from Voyager measurements reported by Tyler *et al.* (1989).

Figure 2. Relationship between tropospheric methane haze opacity and stratospheric haze abundance. Results for three methane bands are shown for 0.20-μm radius stratospheric particles and other stipulated conditions (listed top right). The ethane particulate number density, stratospheric aerosol mass column density (in μg $cm^{-2}$), and stratospheric haze

opacities for each of the wavelengths are depicted by their individual abscissas. Region to the left of the shaded line is ruled out by the physical constraint that opacities do not increase with wavelength (8900 Å opacities exceed 7270 Å opacities by more than 0.013, the uncertainty limit, in this region). Standard model (SM2) values and error bars, derived in Figure 3, are shown with the error bar minima here truncated to reflect the opacity constraint.

Figure 3. Standard deviation, in fractional units, $\sigma_F$, between observed and modelled center-to-limb profiles as a function of stratospheric haze abundance. Results for three methane filters are shown for 0.2-μm radius stratospheric particles for the stratospheric methane mixing ratio and tropospheric hazetop assumptions depicted in the legend. For each wavelength, the radius of curvature of $\sigma_F$ vs the stratospheric number density of ethane particulates (or, alternatively, the stratospheric haze mass column abundance, *c.f.*, alternate axes), is used via Eq. 1 in the text to determine the standard deviation of the haze number density and mass column abundance. The composite best fit value and standard deviation derived from the weighted values of the individual filter standard deviations are shown (circle with error bar). The best fit is designated SM2, one of three standard models.

Figure 4. Constraints on the stratospheric aerosol mass abundances and opacities for three methane mixing ratios. Constraints from center-to-limb profile analysis of the 6190-Å band (dots and error bars representing nominal and 1-$\sigma$ values), 8900-Å profile analysis (dashed lines), and the physical constraint that opacities do not increase with wavelength (solid

hatched curve) restrict the plausible stratospheric aerosol opacity and mass abundance to the regions shown (shaded), as a function of tropospheric hazetop pressure ($P_H$). Stratospheric mass abundance < 0.7 μg cm$^{-2}$ and opacities < 0.06 are indicated, with preferred values (*c.f.*, baseline standard model SM2 for nominal $f_{CH_4,S}$ = 0.00035, panel b) near 0.2 μg cm$^{-2}$ and ~ 0.02.

Figure 5. Constraints on the tropospheric aerosol opacity for three methane mixing ratios. Constraints from center-to-limb profile analysis of the 6190-Å band (dots and error bars representing nominal and 1-$\sigma$ values), 8900-Å profile analysis (dashed lines), and the physical constraint that opacities do not increase with wavelength (solid hatched curve) restrict the plausible stratospheric aerosol opacity and mass abundance to the regions shown (shaded), as a function of tropospheric hazetop pressure ($P_H$). Haze opacity 0.064 - 0.098 is indicated, with preferred values (*c.f.*, baseline standard model SM2, panel B) near 0.085.

Figure 6. Tropospheric methane haze column mass abundances. Shown are constraints as a function of methane haze particle size, as derived from the center-to-limb (CTL) analysis of 6190-Å, 7270-Å, and 8890-Å bands. The error bars depict the range of values derived from matching the CD reflectivity in each of the three methane bands, where each methane band value is weighted by the standard deviation of the modelled/observed CTL profile. The error bars include as well the 3% I/F calibration uncertainty. Best-fit (smallest uncertainty) particle size of 2.5 μm yields a methane mass column abundance 7.81 ± 1.09 μg cm$^{-2}$. Over all plausible particle sizes from 0.2 to 4.0 μm, column abundances of 4 - 11

$\mu g\ cm^{-2}$ are possible.

Figure 7. Limits on the maximum methane haze opacity at 6190-Å. For three stratospheric aerosol sizes (0.15, 0.20, and 0.30 μm), the limits as a function of stratospheric methane mixing ratio are shown for a variety of tropospheric hazetop pressures (0.14, 0.34, and 0.54 bars). Two kinds of limits are depicted: (1) the stratospheric "hazeless limit" where the stratospheric haze disappears (zero opacity), and (2) the limit beyond which the tropospheric $CH_4$ haze opacity violates the optical condition that aerosol opacity not increase substantially with wavelength. Regions to the right of vertical lines in lower right of diagram demand physically unreasonable 7270-Å opacities less than 0.0; they are thus ruled out as unphysical. Together, these conditions imply a maximum tropospheric methane haze opacity less than 0.10 for all particle sizes, hazetop pressures, and stratospheric methane mixing ratios.

Figure 8. Limits on the maximum methane haze opacity at 8900-Å, as a function of stratospheric methane mixing ratio, for 0.20-μm stratospheric particles. Limits depicted are as in Figure 7. The horizontal line in lower right is the 8900-Å opacity limit of 0.013 pertaining to a 7270-Å opacity limit of 0.0; dashed curves below this line are thus ruled out as unphysical. A maximum tropospheric methane haze opacity less than 0.064 is indicated, with a lower limit of 0.013 for all hazetop pressures and stratospheric methane mixing ratios.

Figure 9. Examples of best-fit center-to-limb model profiles for various stratospheric methane mixing ratios. Curves pertain to a methane hazetop of 0.34 bars. Both stratospheric and tropospheric haze opacities were adjusted to obtain the best-fit curves shown for each value of the stratospheric gaseous methane abundance.

Figure 10. Standard deviation, in fractional units, $\sigma_F$, between observed and modelled center-to-limb profiles as a function of stratospheric methane mixing ratio $f_{CH_4,S}$ Radius of curvature of $\sigma_F$ vs $f_{CH_4,S}$ is used to determine the standard deviation of $f_{CH_4,S}$.

Figure 11. Stratospheric gaseous methane mixing ratio ($f_{CH_4,S}$) vs tropospheric methane hazetop pressure ($P_H$), for $\langle r_s \rangle$ = 0.2 μm. Center-to-limb (CTL) behavior of 8900-Å and 7270-Å methane absorption, as quantified by standard deviations between model and observations (*c.f.* Figure 10), yields primary limits (thick) and nominal values (thick dashed). Other constraints result from analysis of the methane haze opacities required to produce satisfactory CTL fits. Large $CH_4$ mixing ratios (> 0.002) require unphysical 7270-Å opacities < 0, and thus are ruled out. Also depicted is the maximum pressure which satisfying the nominal 6190 Å data as well as the $\tau$(8900 Å) > $\tau$(7270 Å) constraint. Analysis indicates $f_{CH_4,S} < 0.0017$, with a preferred range $2\ 10^{-5}$ - $10^{-3}$ satisfying the nominal 6190 Å CD reflectivity as well as the 7270 Å and 8900 Å constraints. A tropospheric methane hazetop pressure $0.1 < P_H < 0.65$ bars is indicated, with a preferred range $0.1 < P_H < 0.52$ bars. Standard models chosen to analyze optical properties of various aerosol layers are indicated (SM1, SM2, and SM3). SM2 is the best-fit nominal model, with $P_H$ =

0.34 bar and $f_{CH_4,S}$ = 0.00035. This is the $f_{CH_4,S}$ predicted for a tropopause temperature of 56 K (upper scale), well within the spatially-varying range of coldtrap temperatures reported by Conrath, Flaser, and Gierasch (1991a; labelled CFG in diagram), and indicates that convective upwelling of tropospheric methane may not be required. The tropopause temperature of Lindal (1992), is depicted (L), as are the ranges of $f_{CH_4,S}$ reported by Bishop *et al.* (1992), Orton *et al.* (1992), and Yelle *et al.* (1993).

Figure 12. Nominal atmospheric structure for Neptune's Equatorial Region. Parameters for the baseline standard model, SM2, are depicted. For the $CH_4$ haze, parameter values for two types of particles are shown: (1) 2.5-μm Mie scatterers, and (2) particles adopting the nominal double Henyey-Greenstein phase function parameters empirically derived from Voyager multiple phase-angle observations (Pryor *et al.*, 1992). Bottom cloud pressure is from Baines and Smith (1990). The thermal profile reported by the Voyager Radio Subsystem (RSS) occultation experiment (Tyler *et al.*, 1989) is shown with an adiabatic extrapolation into the deep atmosphere. Mixing ratios of Baines and Smith (1990) are adopted for tropospheric methane ($f_{CH_4}$) and for the fraction of hydrogen in the equilibrium state ($f_{eH_2}$).

Figure 13. Baseline standard model (SM2) center-to-limb profiles (curves) compared to the observations (dots). Standard deviations of the model fit curves, in I/F units, are listed under the wavelengths.

Figure 14. Nominal, SM2-model opacities for various hydrocarbon layers within Neptune's Equatorial Region. $CH_4$ haze opacity curve assumes Mie scattering with $<r> = 2.5$ μm. Individual points and error bars, accounting for the 3% calibration uncertainty of the data, indicate the $CH_4$ haze opacity constraints derived utilizing the nominal Pryor *et al.* (1992) double Henyey-Greenstein phase function. Opacities are less than 0.1 in both the stratosphere and troposphere throughout the visible.

Figure 15. Bottom cloud single-scattering albedo shows marked absorption in the red and near-infrared, in both imagery of the Equatorial Region and spectroscopy of the entire globe. Results of Baines and Smith (1990) and Pryor *et al.* (1992) are also indicated. A parameterized fit to the 6340-Å and 8260-Å points (curve; following, for example, Baines and Bergstralh, 1986) yields the formula shown, for use in modelling continuous spectra (*c.f.*, Figure 17).

Figure 16. Ultraviolet imaginary refractive index/single-scattering albedo from global IUE observations. Shown are the indices required for stratospheric aerosols to match the relatively-dark IUE geometric albedos at 2000 Å and 2600 Å (nominally, thick and thin dot-dashed, respectively). The nominal Equatorial Region (ER) model (SM2) can not match the 2000-Å geometric albedo, even with large $n_i$, thus indicating that this region is markedly depleted in stratospheric aerosols compared to the global average. Results for the global model, with 7.7 times the nominal ER stratospheric aerosol abundance, as derived from fitting the 8900-Å band (*c.f.*, Figure 17), are also shown (vertical dashed), together with the

Pryor *et al.* (1992) model results derived from 2650-Å Voyager PPS observations. Reasonable UV imaginary indices ($n_i < 0.03$) are derived by both investigations.

Figure 17. Equatorial Region (ER) and global model fits to the geometric albedo spectrum, 7700-10000 Å. Open points with associated "error bars" show the calculated geometric albedos and filter band width pertaining to the 8260-Å, and 8900-Å ER center-to- limb profiles. They indicate the geometric albedo which the planet would exhibit if it had the ER aerosol structure across the disk. At all wavelengths, the global spectrum is brighter than that predicted from the ER structure, indicating enhanced aerosol scattering. Deep 8900-Å band global narrow-band spectrum is satisfied by the global model incorporating 7.7 times the high-altitude scattering haze burden ($m_s$) of the ER model. Modelled spectrum utilizing bottom cloud single-scattering albedos as parameterized from 6340-Å and 8260-Å data (*c.f.*, Figure 15) is too dark near 9400 Å (dashed curve). This pseudo-continuum region indicates an increase in single-scattering in the near-infrared. Neither the ER nor global models fit the $S_3(0)$ pressure-induced region near 8300-Å.

Figure 18. Model fits to the $S_3(0)$ region. Models shown are for enhanced methane haze opacity (thick curve) and a near-normal *ortho/para* hydrogen distribution (thin curve; $f_{eH_2}$ = 0.14 means that $1\text{-}f_{eH_2}$ = 0.86 of the hydrogen is in the normal state). Both models satisfy the psuedo-continuum and nearby 8260-Å peak $H_2$ absorption satisfactorily. However, the enhanced methane haze model is excessively bright in intermediate bands.

Figure 19. Fit of 22-30° S 7500-Å PPS data to modified model structures proposed in this paper (including stratospheric methane mixing ratio of 0.00035 and hazetop pressure of 0.34 bars). Satisfactory fits to both the nominal global (A) and Equatorial Region (B) models are found for low phase angle data when the methane haze opacity is increased to 0.24 - 0.34 from ~ 0.05. Excessive forward scattering by stratospheric hazes for this modified global model causes unsatisfactory fits to high phase observations. More satisfactory fits are found for the optically-thinner Equatorial Region model, which then violates the UV constraint (*c.f.*, Figure 16). 1A re-analysis of phase function parameters for high phase angles is suggested.

FIGURE 1

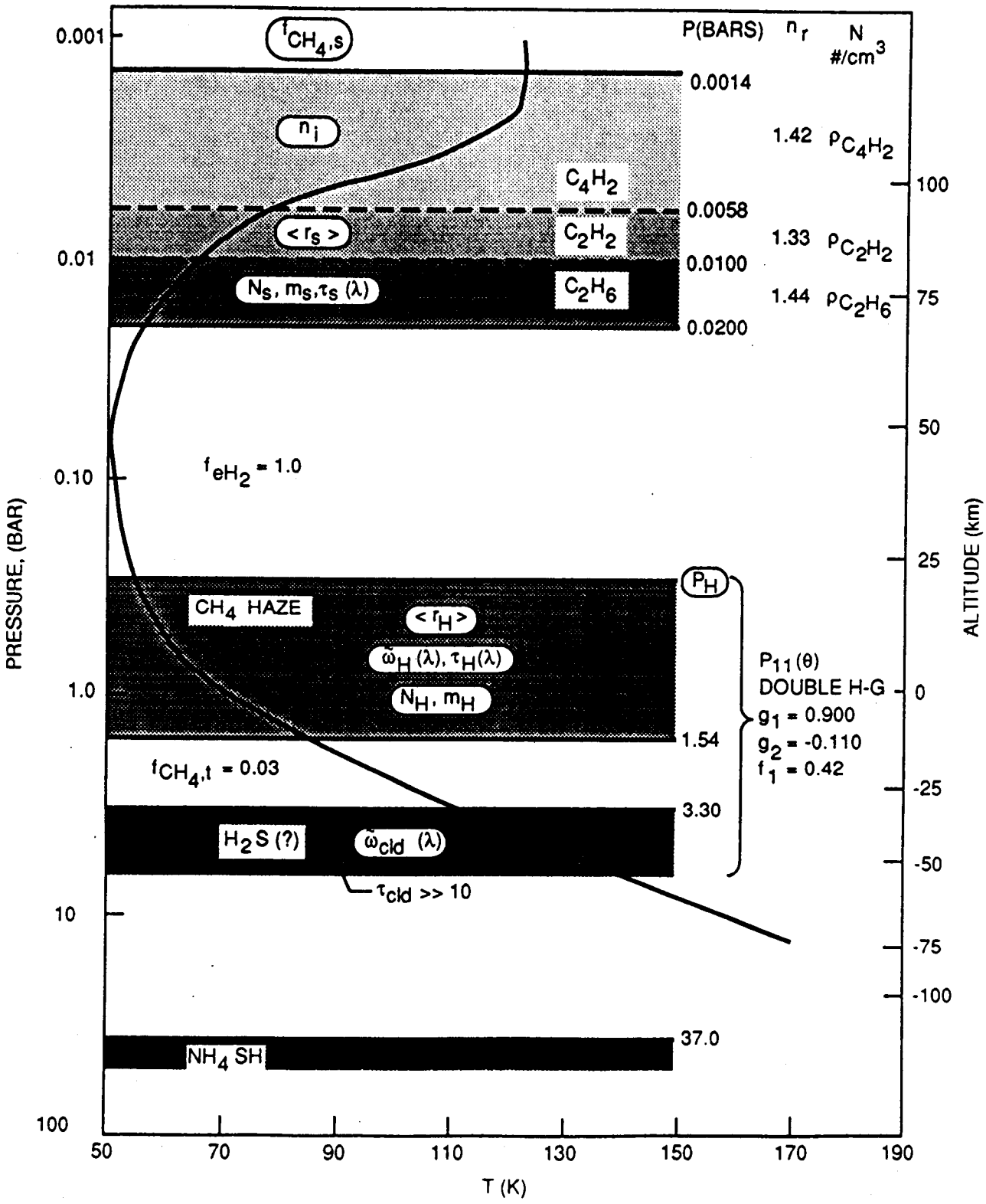
0.001
0.01
0.10
1.0
10
100
PRESSURE, (BAR)
$f_{CH_4,s}$
P(BARS)
$n_r$
N #/cm$^3$
0.0014
$n_i$
1.42 $\rho_{C_4H_2}$
$C_4H_2$
0.0058
$< r_s >$
$C_2H_2$
1.33 $\rho_{C_2H_2}$
0.0100
$N_s, m_s, \tau_s(\lambda)$
$C_2H_6$
1.44 $\rho_{C_2H_6}$
0.0200
$f_{eH_2} = 1.0$
$P_H$
$CH_4$ HAZE
$< r_H >$
$\tilde{\omega}_H(\lambda), \tau_H(\lambda)$
$N_H, m_H$
$P_{11}(\theta)$
DOUBLE H-G
$g_1 = 0.900$
$g_2 = -0.110$
$f_1 = 0.42$
1.54
$f_{CH_4,t} = 0.03$
3.30
$H_2S$ (?)
$\tilde{\omega}_{cld}(\lambda)$
$\tau_{cld} >> 10$
37.0
$NH_4SH$
100
75
50
25
0
-25
-50
-75
-100
ALTITUDE (km)
50
70
90
110
130
150
170
190
T (K)

FIGURE 2

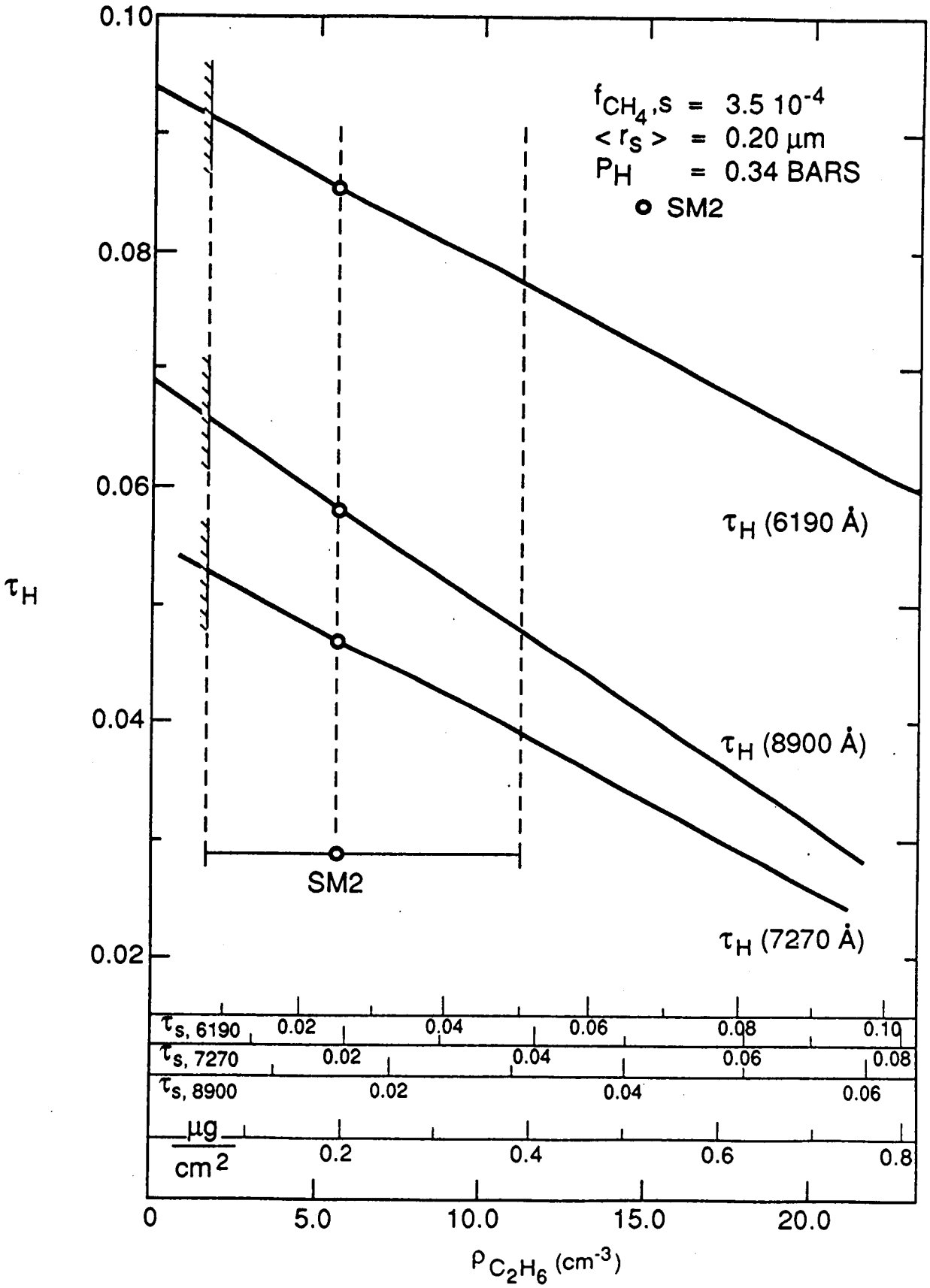
0.10
0.08
0.06
0.04
0.02
$\tau_H$
$f_{CH_4,s}$ = 3.5 $10^{-4}$
$< r_s >$ = 0.20 μm
$P_H$ = 0.34 BARS
SM2
$\tau_H$ (6190 Å)
$\tau_H$ (8900 Å)
$\tau_H$ (7270 Å)
SM2
$\tau_{s,6190}$ 0.02 0.04 0.06 0.08 0.10
$\tau_{s,7270}$ 0.02 0.04 0.06 0.08
$\tau_{s,8900}$ 0.02 0.04 0.06
$\frac{\mu g}{cm^2}$ 0.2 0.4 0.6 0.8
0 5.0 10.0 15.0 20.0
$\rho_{C_2H_6}$ ($cm^{-3}$)

FIGURE 3

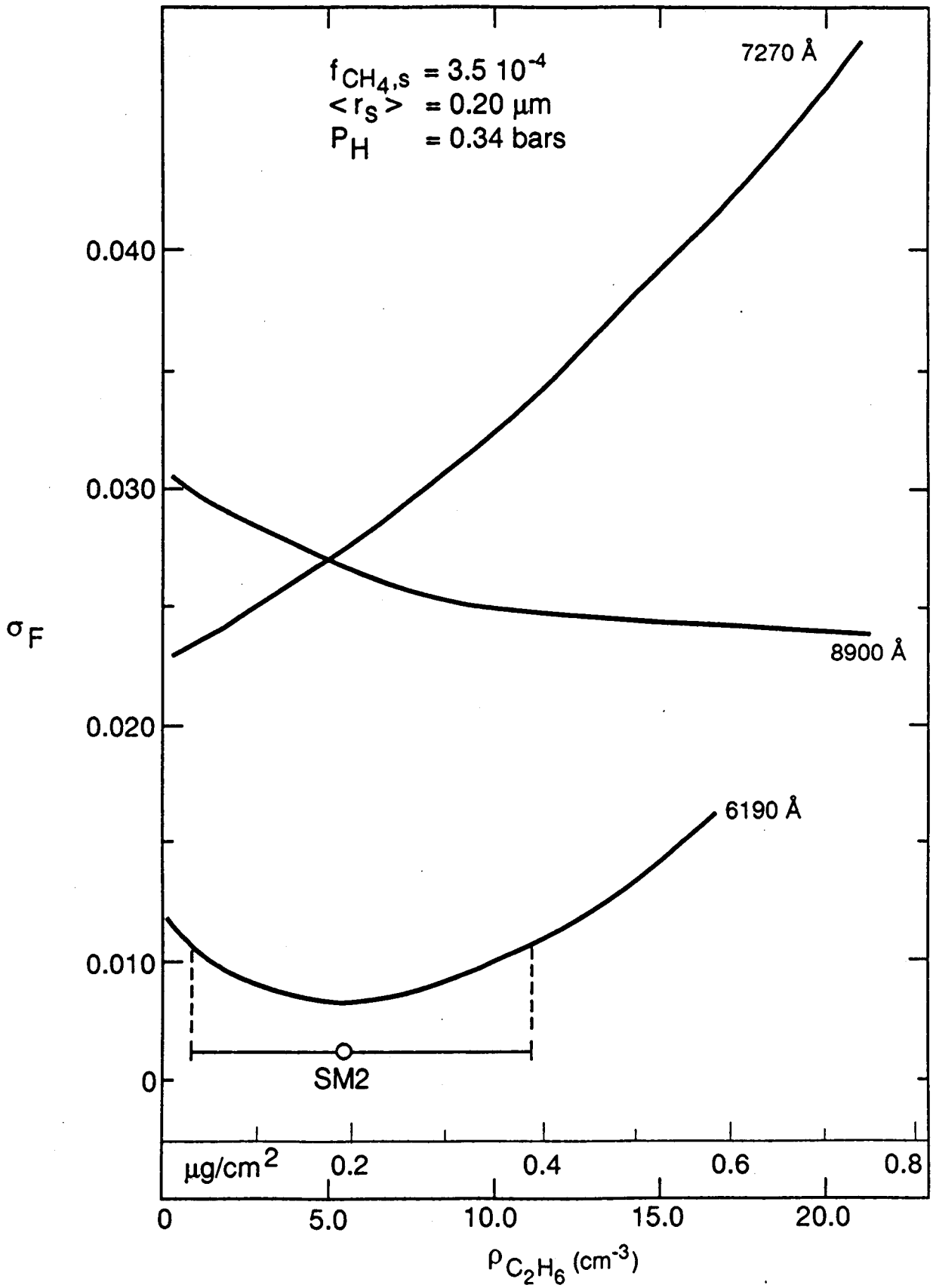
$f_{CH_4,s}$ = 3.5 $10^{-4}$
$<r_s>$ = 0.20 µm
$P_H$ = 0.34 bars
7270 Å
8900 Å
6190 Å
SM2
$\sigma_F$
0.040
0.030
0.020
0.010
0
µg/cm$^2$
0.2
0.4
0.6
0.8
0
5.0
10.0
15.0
20.0
$\rho_{C_2H_6}$ (cm$^{-3}$)

FIGURE 4

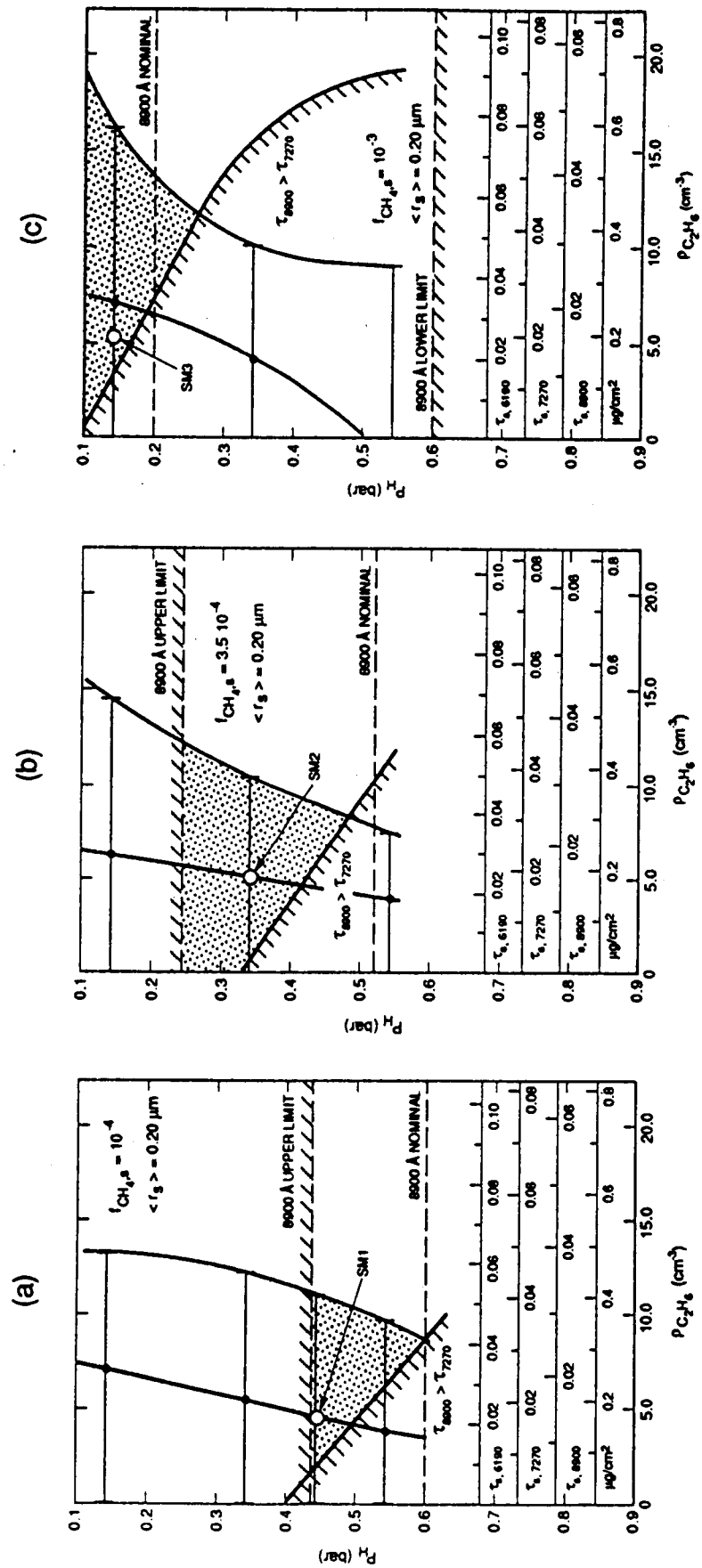
(a)
(b)
(c)
8900 Å NOMINAL
8900 Å UPPER LIMIT
8900 Å LOWER LIMIT
SM1
SM2
SM3
$f_{CH_4,s} = 10^{-4}$
$f_{CH_4,s} = 3.5\ 10^{-4}$
$f_{CH_4,s} = 10^{-3}$
$< r_s > = 0.20\ \mu m$
$\tau_{8900} > \tau_{7270}$
$P_H$ (bar)
$\rho_{C_2H_6}$ ($cm^{-3}$)
$\tau_{s,6190}$
$\tau_{s,7270}$
$\tau_{s,8900}$
$\mu g/cm^2$

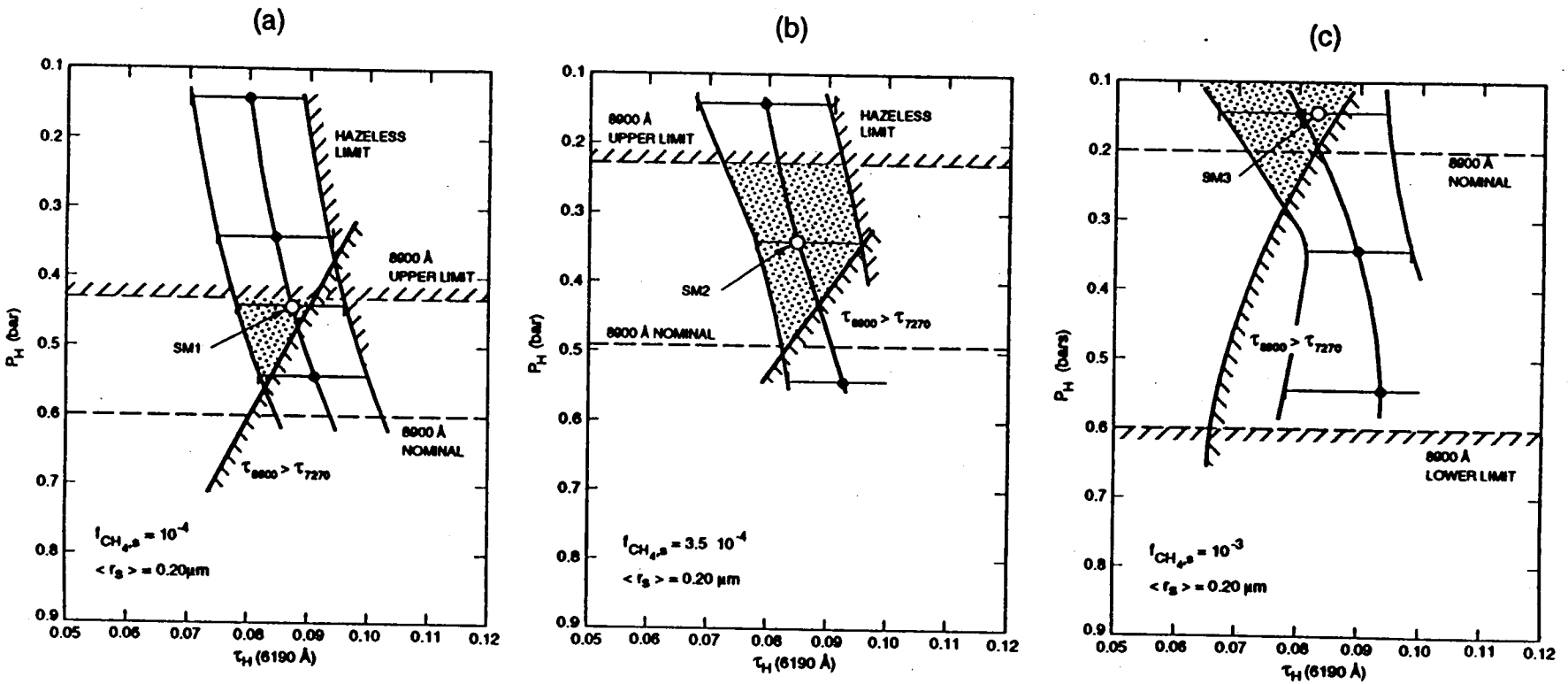
(a)
HAZELESS LIMIT
8900 Å UPPER LIMIT
SM1
8900 Å NOMINAL
$\tau_{8900} > \tau_{7270}$
$f_{CH_4,s} = 10^{-4}$
$< r_s > = 0.20 \mu m$
$P_H$ (bar)
$\tau_H$ (6190 Å)
(b)
8900 Å UPPER LIMIT
HAZELESS LIMIT
SM2
8900 Å NOMINAL
$\tau_{8900} > \tau_{7270}$
$f_{CH_4,s} = 3.5\ 10^{-4}$
$< r_s > = 0.20\ \mu m$
$P_H$ (bar)
$\tau_H$ (6190 Å)
(c)
SM3
8900 Å NOMINAL
$\tau_{8900} > \tau_{7270}$
8900 Å LOWER LIMIT
$f_{CH_4,s} = 10^{-3}$
$< r_s > = 0.20\ \mu m$
$P_H$ (bars)
$\tau_H$ (6190 Å)

FIGURE 5

FIGURE 6

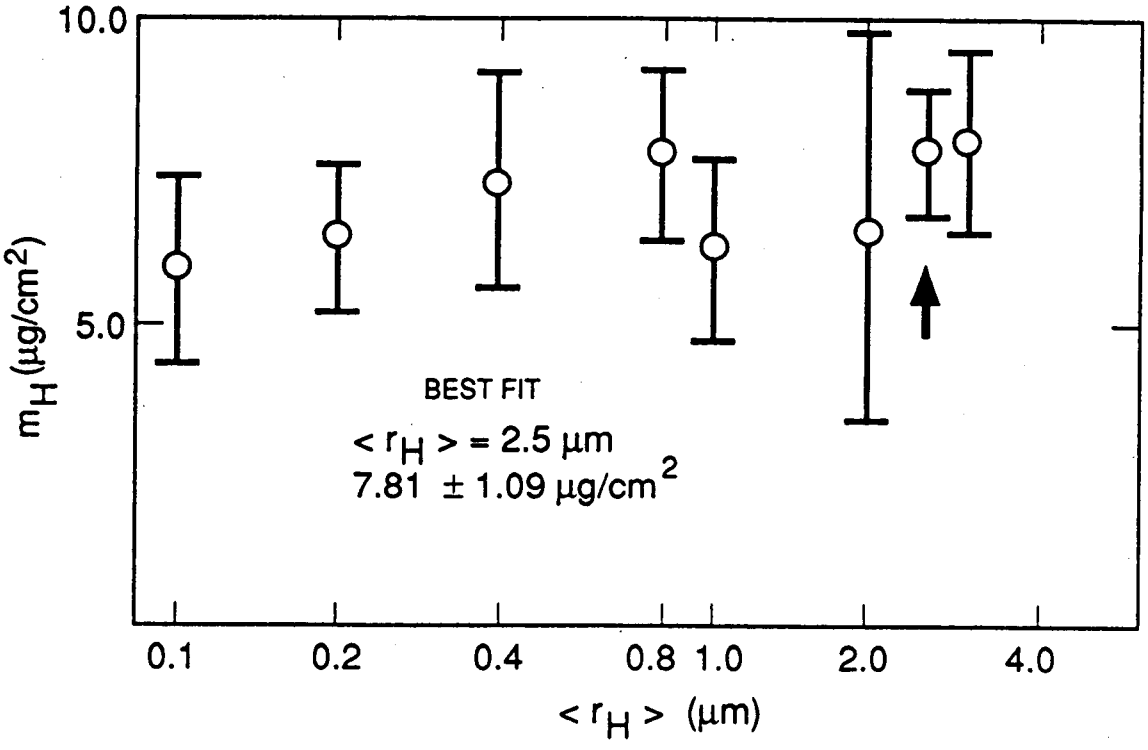
10.0
5.0
$m_H$ (μg/cm$^2$)
BEST FIT
< $r_H$ > = 2.5 μm
7.81 ± 1.09 μg/cm$^2$
0.1
0.2
0.4
0.8
1.0
2.0
4.0
< $r_H$ > (μm)

FIGURE 7

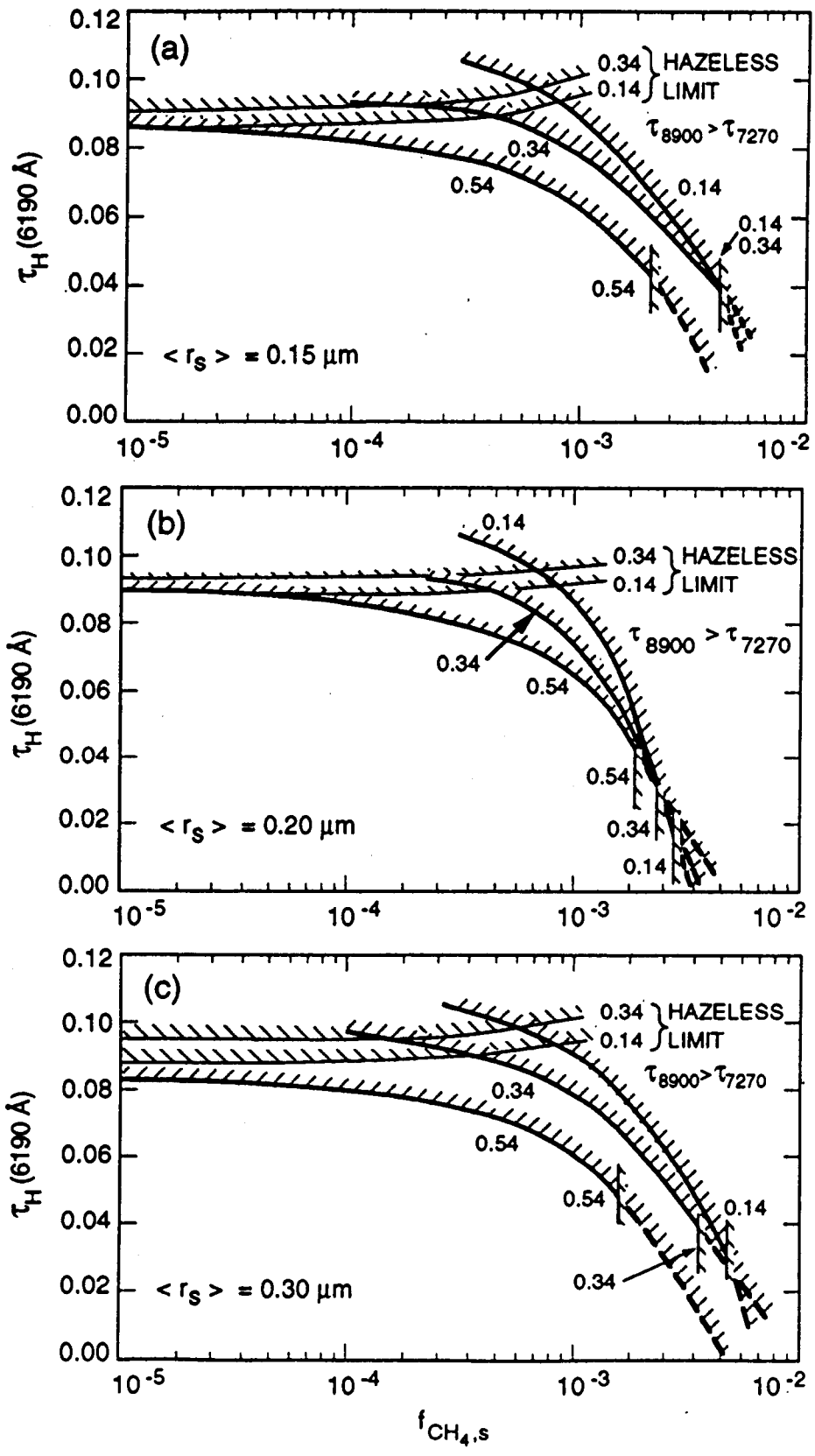
(a)
0.34 } HAZELESS
0.14 } LIMIT
$\tau_{8900} > \tau_{7270}$
0.34
0.54
0.14
0.14
0.34
0.54
$< r_s > = 0.15\ \mu m$
(b)
0.14
0.34 } HAZELESS
0.14 } LIMIT
$\tau_{8900} > \tau_{7270}$
0.34
0.54
0.54
0.34
0.14
$< r_s > = 0.20\ \mu m$
(c)
0.34 } HAZELESS
0.14 } LIMIT
$\tau_{8900} > \tau_{7270}$
0.34
0.54
0.54
0.14
0.34
$< r_s > = 0.30\ \mu m$
$\tau_H$(6190 Å)
0.12
0.10
0.08
0.06
0.04
0.02
0.00
$10^{-5}$
$10^{-4}$
$10^{-3}$
$10^{-2}$
$f_{CH_4,s}$

FIGURE 8

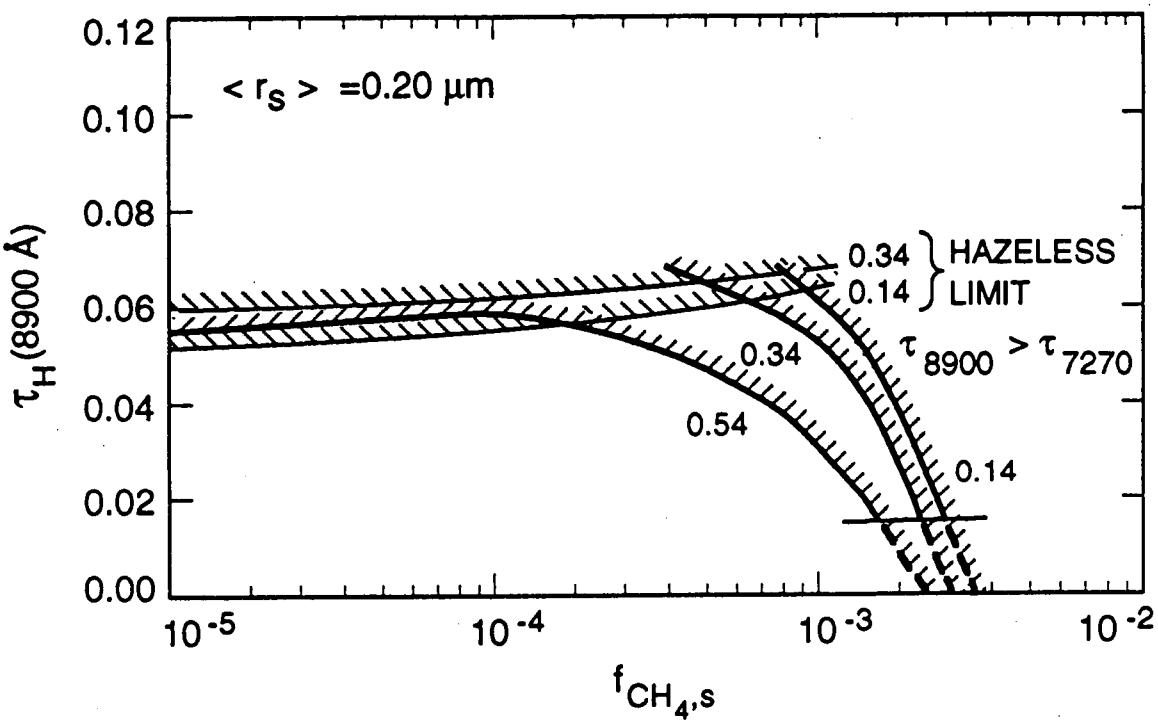
0.12
0.10
0.08
0.06
0.04
0.02
0.00
$\tau_H$(8900 Å)
$< r_s >$ =0.20 μm
0.34
0.14
HAZELESS LIMIT
$\tau_{8900} > \tau_{7270}$
0.34
0.54
0.14
$10^{-5}$
$10^{-4}$
$10^{-3}$
$10^{-2}$
$f_{CH_4,s}$

FIGURE 9

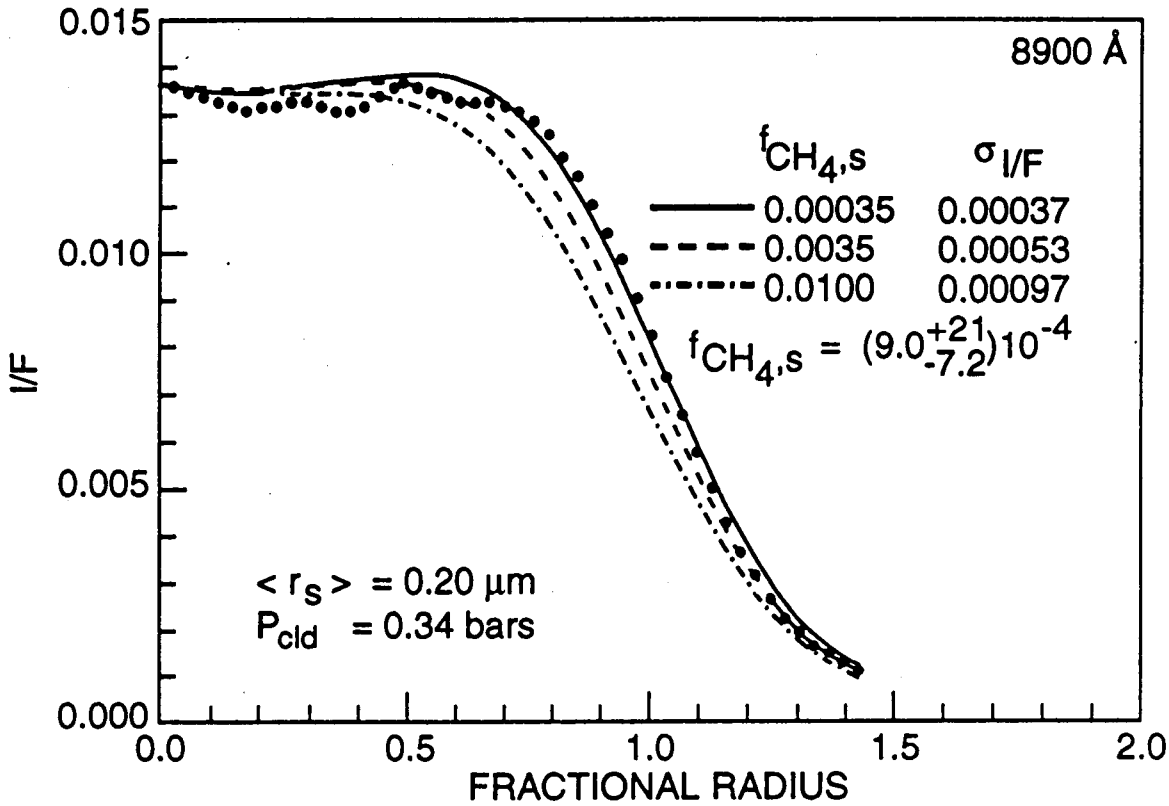
0.015
0.010
0.005
0.000
I/F
0.0
0.5
1.0
1.5
2.0
FRACTIONAL RADIUS
8900 Å
$f_{CH_4,s}$ $\sigma_{I/F}$
0.00035 0.00037
0.0035 0.00053
0.0100 0.00097
$f_{CH_4,s} = (9.0^{+21}_{-7.2})10^{-4}$
$< r_s > = 0.20\ \mu m$
$P_{cld} = 0.34$ bars

FIGURE 10

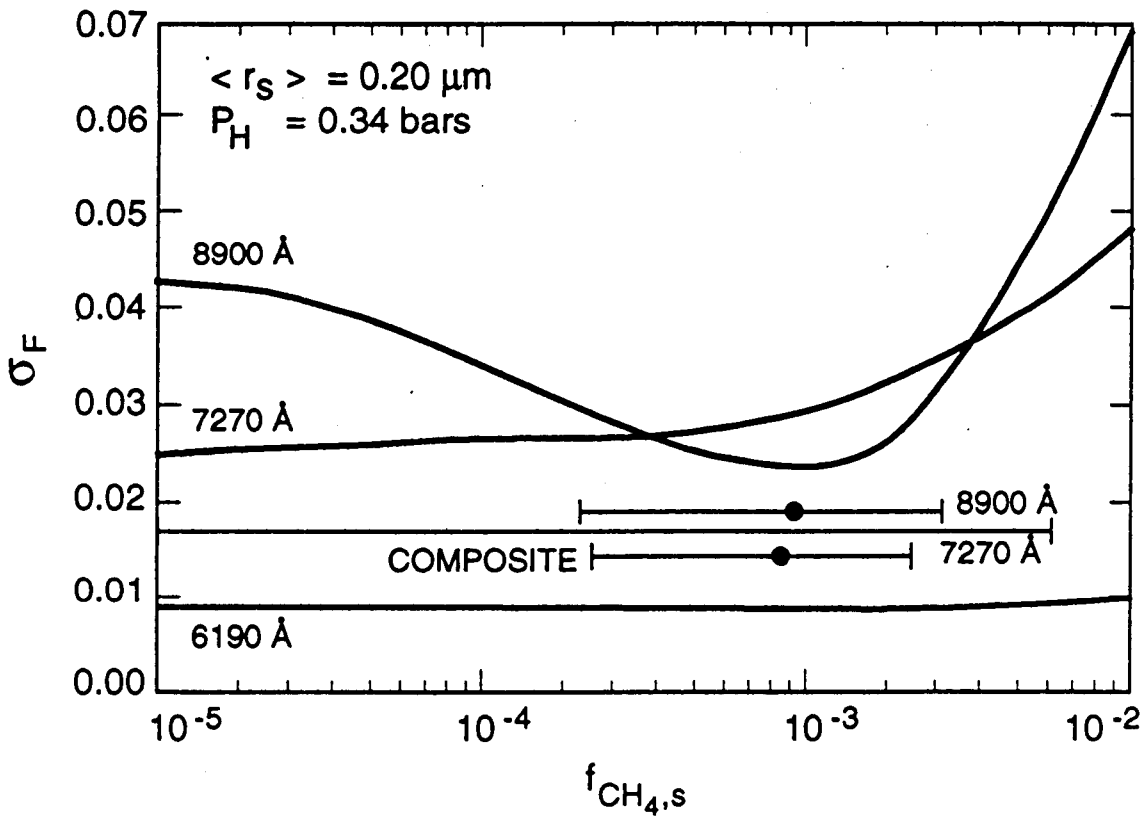
0.07
0.06
0.05
0.04
0.03
0.02
0.01
0.00
$\sigma_F$
$< r_s >$ = 0.20 μm
$P_H$ = 0.34 bars
8900 Å
7270 Å
6190 Å
8900 Å
COMPOSITE
7270 Å
$10^{-5}$
$10^{-4}$
$10^{-3}$
$10^{-2}$
$f_{CH_4,s}$

FIGURE 11

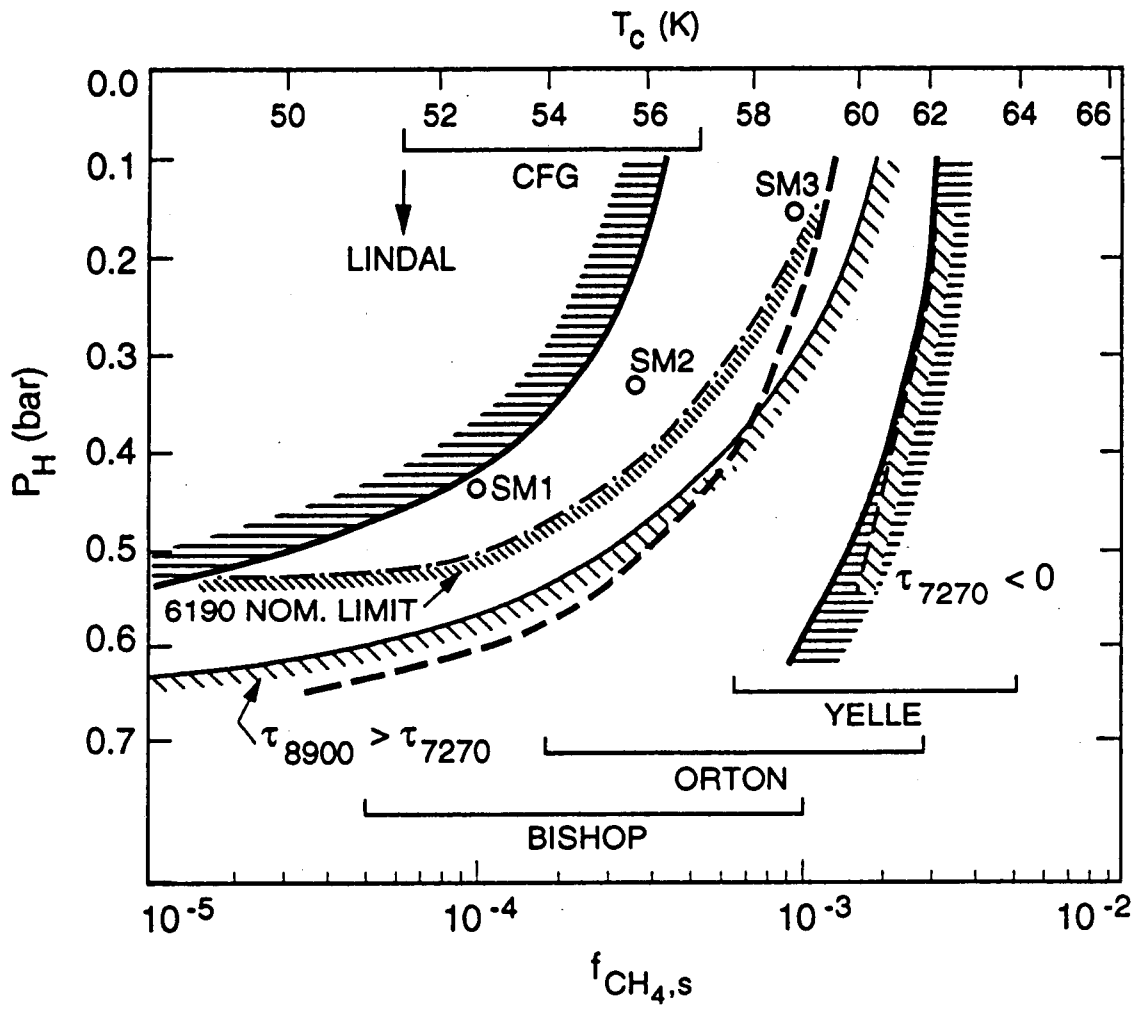
$T_c$ (K)
50
52
54
56
58
60
62
64
66
0.0
0.1
0.2
0.3
0.4
0.5
0.6
0.7
$P_H$ (bar)
CFG
LINDAL
SM1
SM2
SM3
6190 NOM. LIMIT
$\tau_{8900} > \tau_{7270}$
$\tau_{7270} < 0$
YELLE
ORTON
BISHOP
$10^{-5}$
$10^{-4}$
$10^{-3}$
$10^{-2}$
$f_{CH_4,s}$

FIGURE 12

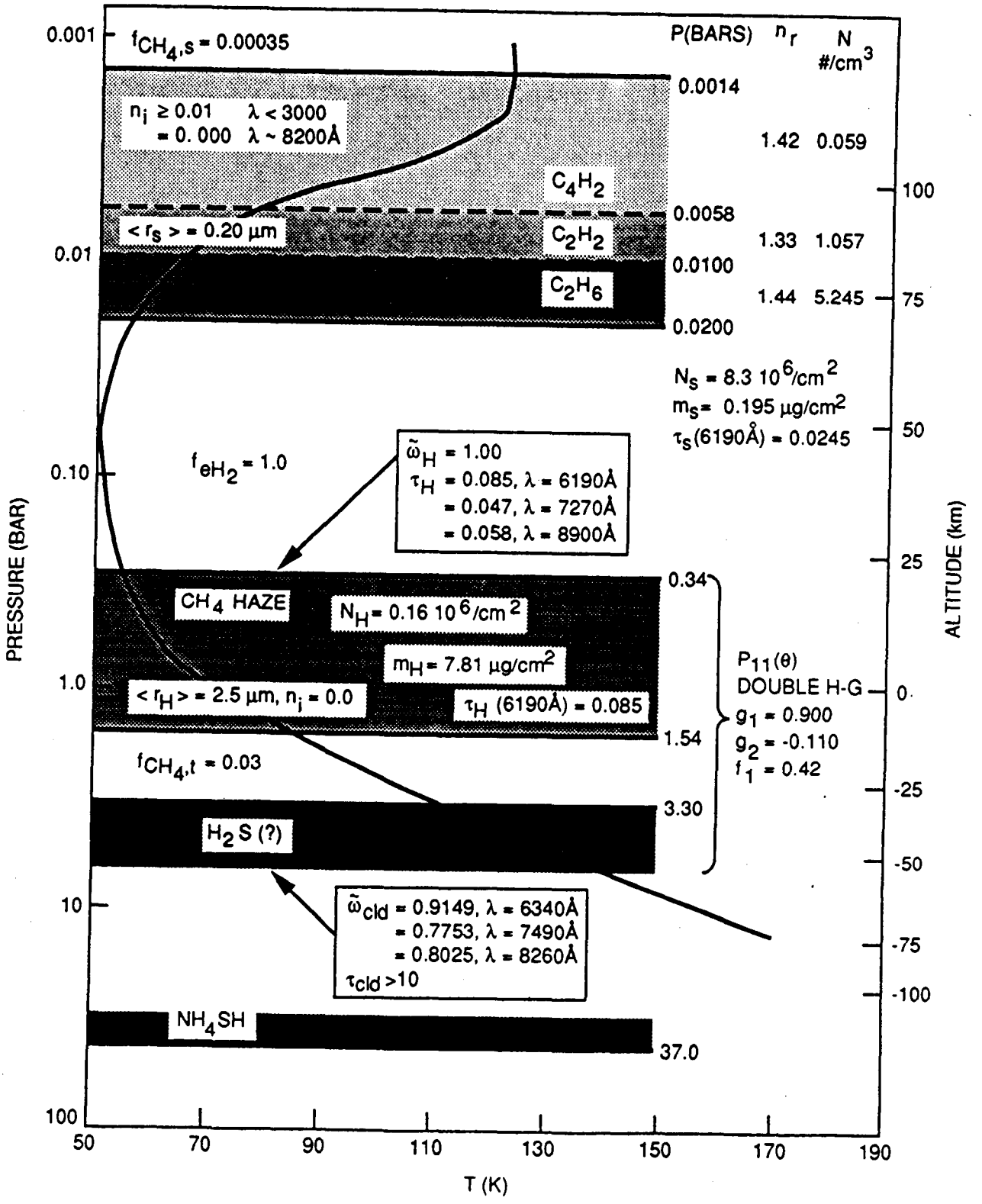
0.001
$f_{CH_4,s}$ = 0.00035
P(BARS)
$n_r$
N #/cm$^3$
$n_i \geq 0.01$ $\lambda < 3000$
= 0. 000 $\lambda \sim 8200$Å
0.0014
1.42 0.059
$C_4H_2$
0.0058
$< r_s >$ = 0.20 µm
$C_2H_2$
1.33 1.057
0.01
0.0100
$C_2H_6$
1.44 5.245
0.0200
$N_s$ = 8.3 10$^6$/cm$^2$
$m_s$= 0.195 µg/cm$^2$
$\tau_s$(6190Å) = 0.0245
$f_{eH_2}$ = 1.0
$\tilde{\omega}_H$ = 1.00
$\tau_H$ = 0.085, $\lambda$ = 6190Å
= 0.047, $\lambda$ = 7270Å
= 0.058, $\lambda$ = 8900Å
0.10
0.34
$CH_4$ HAZE
$N_H$= 0.16 10$^6$/cm$^2$
$m_H$= 7.81 µg/cm$^2$
$< r_H >$ = 2.5 µm, $n_i$ = 0.0
$\tau_H$ (6190Å) = 0.085
1.0
1.54
$P_{11}(\theta)$
DOUBLE H-G
$g_1$ = 0.900
$g_2$ = -0.110
$f_1$ = 0.42
$f_{CH_4,t}$ = 0.03
3.30
$H_2S$ (?)
10
$\tilde{\omega}_{cld}$ = 0.9149, $\lambda$ = 6340Å
= 0.7753, $\lambda$ = 7490Å
= 0.8025, $\lambda$ = 8260Å
$\tau_{cld}$ >10
$NH_4SH$
37.0
100
50
70
90
110
130
150
170
190
T (K)
PRESSURE (BAR)
ALTITUDE (km)
100
75
50
25
0.
-25
-50
-75
-100

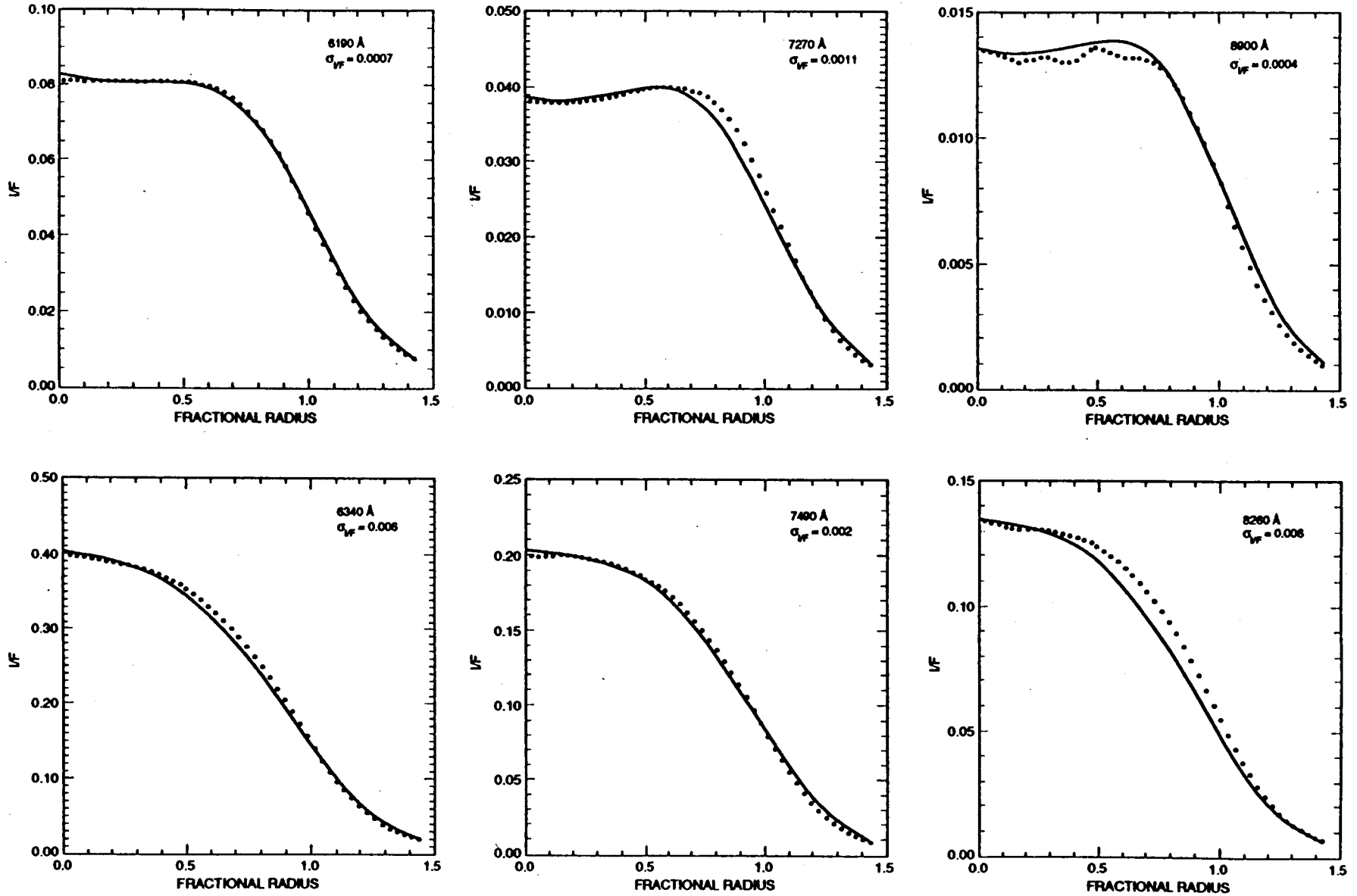
6190 Å
$\sigma_{I/F}$ = 0.0007
7270 Å
$\sigma_{I/F}$ = 0.0011
8900 Å
$\sigma_{I/F}$ = 0.0004
6340 Å
$\sigma_{I/F}$ = 0.006
7490 Å
$\sigma_{I/F}$ = 0.002
8260 Å
$\sigma_{I/F}$ = 0.006
I/F
FRACTIONAL RADIUS

FIGURE 13

FIGURE 14

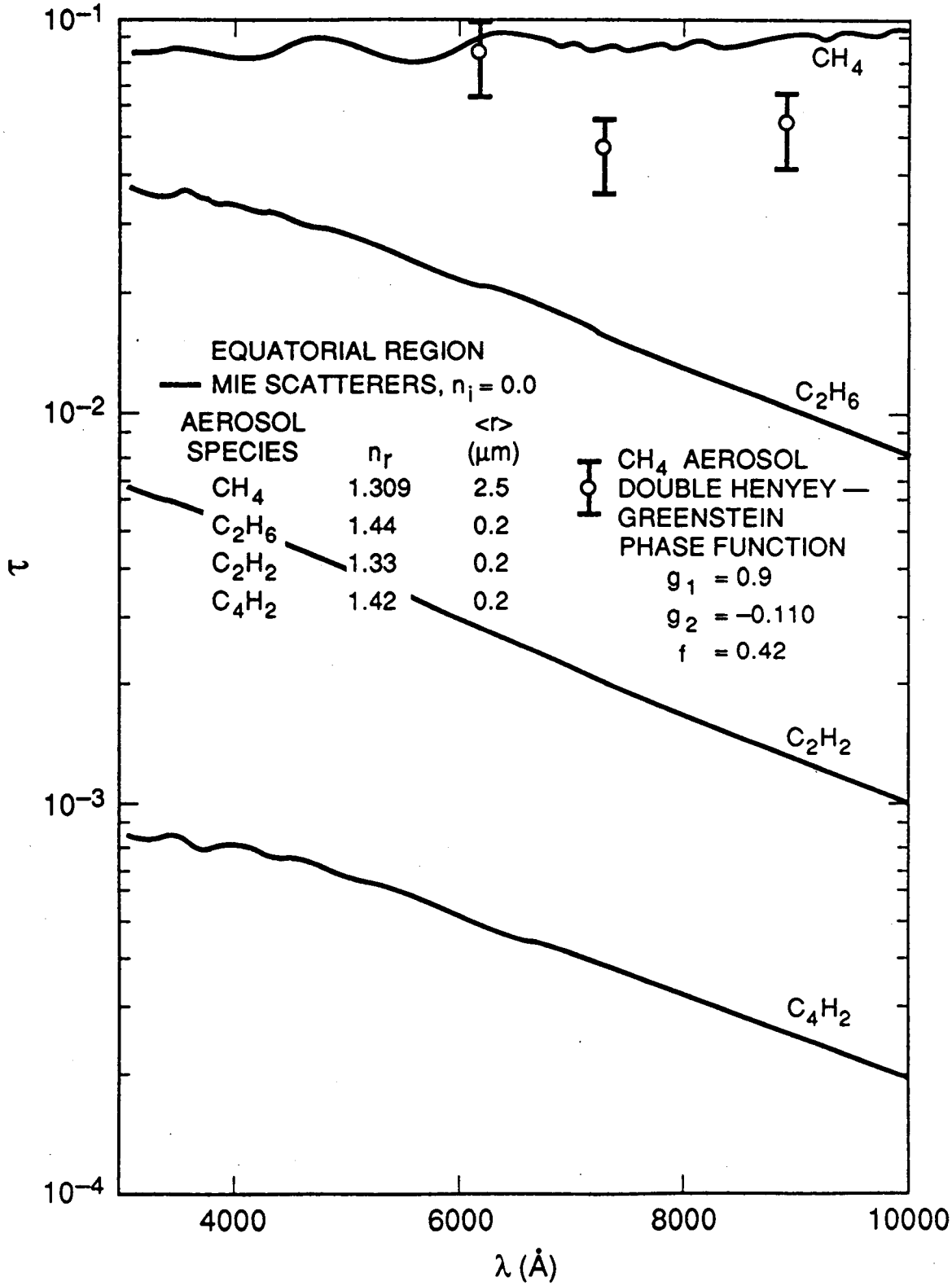
$10^{-1}$
$10^{-2}$
$10^{-3}$
$10^{-4}$
τ
4000
6000
8000
10000
λ (Å)
$CH_4$
$C_2H_6$
$C_2H_2$
$C_4H_2$
EQUATORIAL REGION
MIE SCATTERERS, $n_i = 0.0$
AEROSOL SPECIES
$n_r$
<r> (μm)
$CH_4$ 1.309 2.5
$C_2H_6$ 1.44 0.2
$C_2H_2$ 1.33 0.2
$C_4H_2$ 1.42 0.2
$CH_4$ AEROSOL
DOUBLE HENYEY — GREENSTEIN PHASE FUNCTION
$g_1 = 0.9$
$g_2 = -0.110$
$f = 0.42$

FIGURE 15

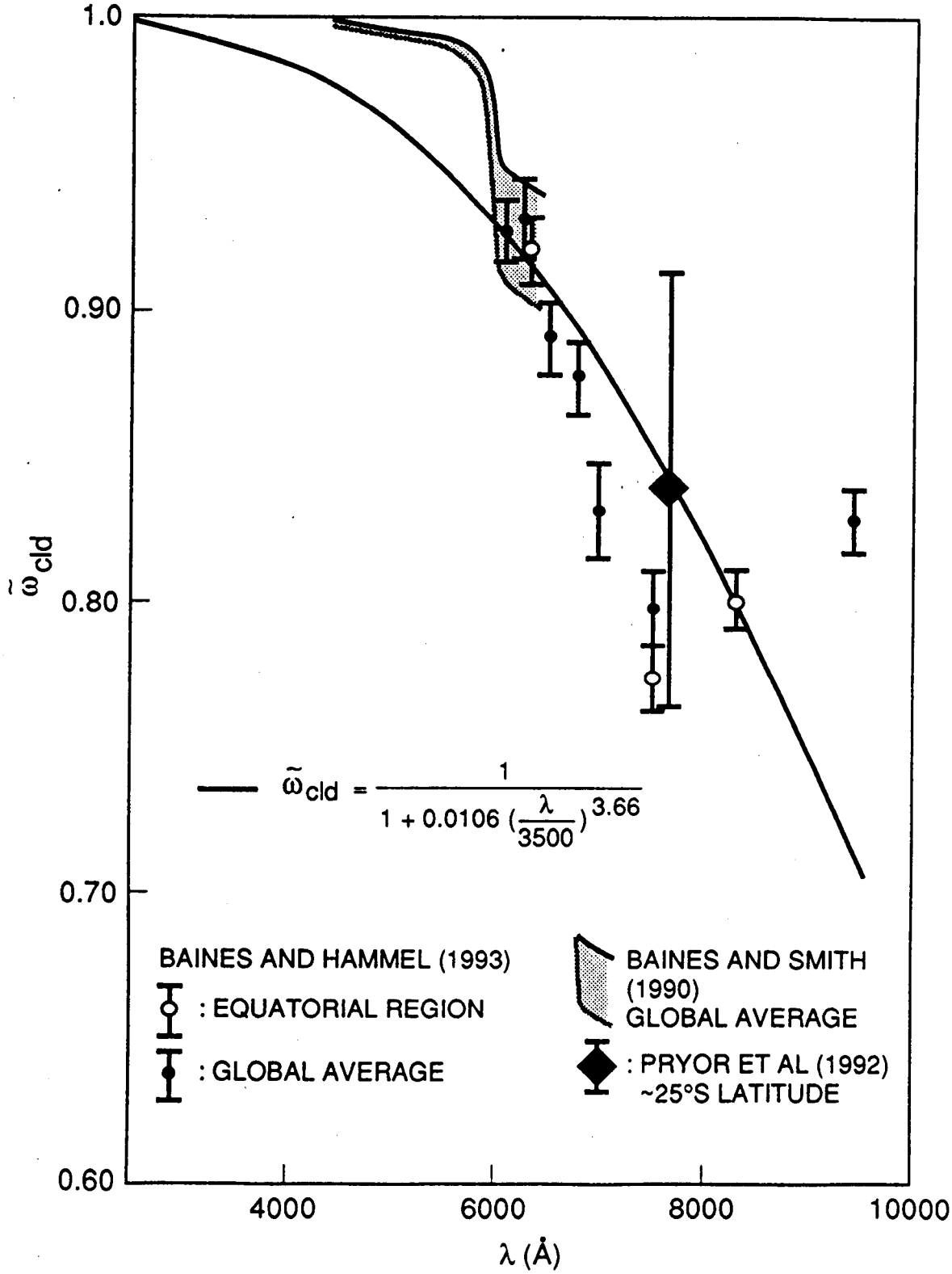
1.0
0.90
0.80
0.70
0.60
$\tilde{\omega}_{cld}$
$\tilde{\omega}_{cld} = \frac{1}{1 + 0.0106\,(\frac{\lambda}{3500})^{3.66}}$
BAINES AND HAMMEL (1993)
: EQUATORIAL REGION
: GLOBAL AVERAGE
BAINES AND SMITH (1990) GLOBAL AVERAGE
: PRYOR ET AL (1992) ~25°S LATITUDE
4000
6000
8000
10000
λ (Å)

FIGURE 16

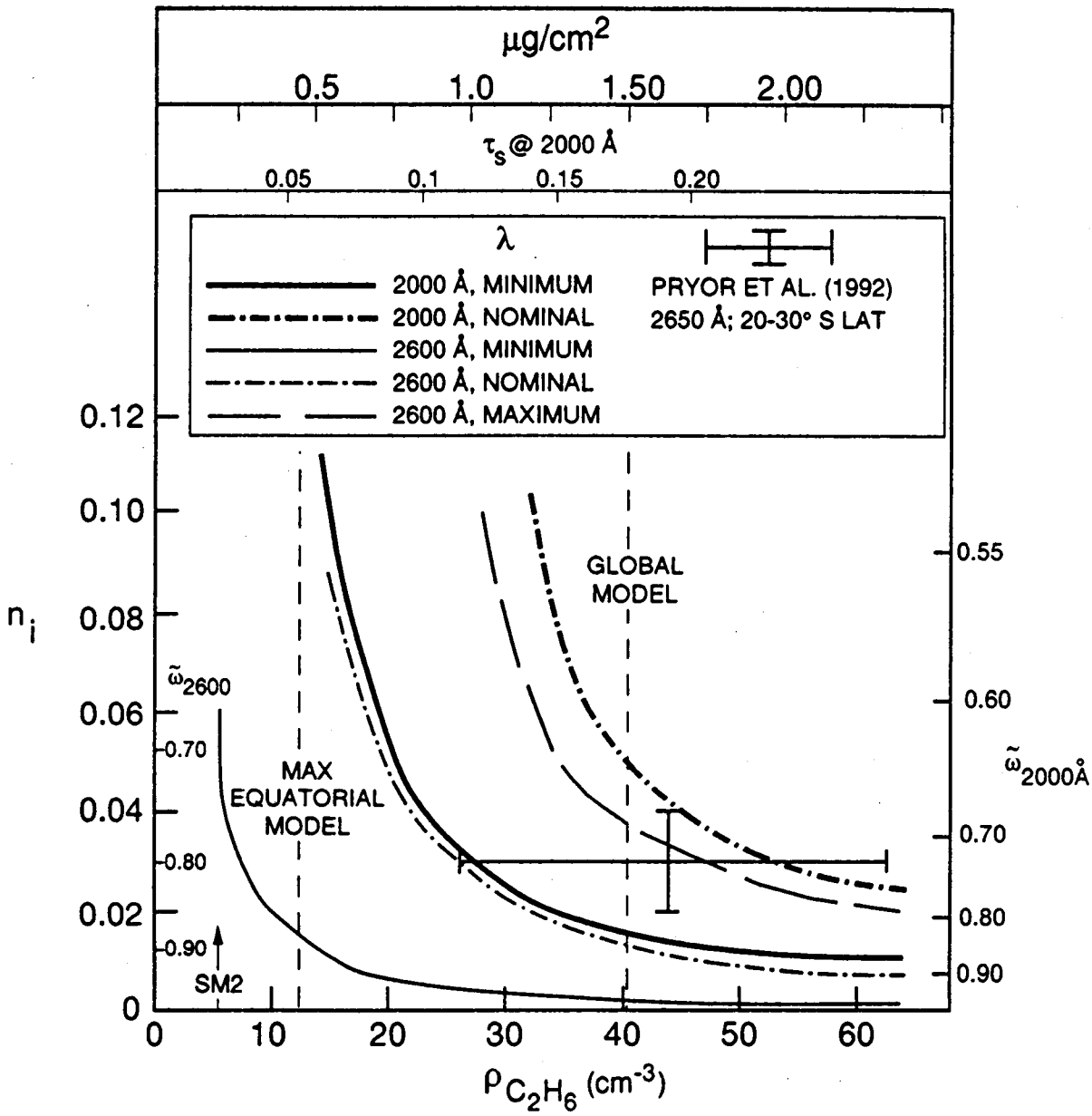
μg/cm²
0.5
1.0
1.50
2.00
τs @ 2000 Å
0.05
0.1
0.15
0.20
λ
2000 Å, MINIMUM
2000 Å, NOMINAL
2600 Å, MINIMUM
2600 Å, NOMINAL
2600 Å, MAXIMUM
PRYOR ET AL. (1992)
2650 Å; 20-30° S LAT
GLOBAL MODEL
MAX EQUATORIAL MODEL
SM2
ni
ω̃2600
ω̃2000Å
0.12
0.10
0.08
0.06
0.04
0.02
0
0.70
0.80
0.90
0.55
0.60
0.70
0.80
0.90
0
10
20
30
40
50
60
ρC2H6 (cm-3)

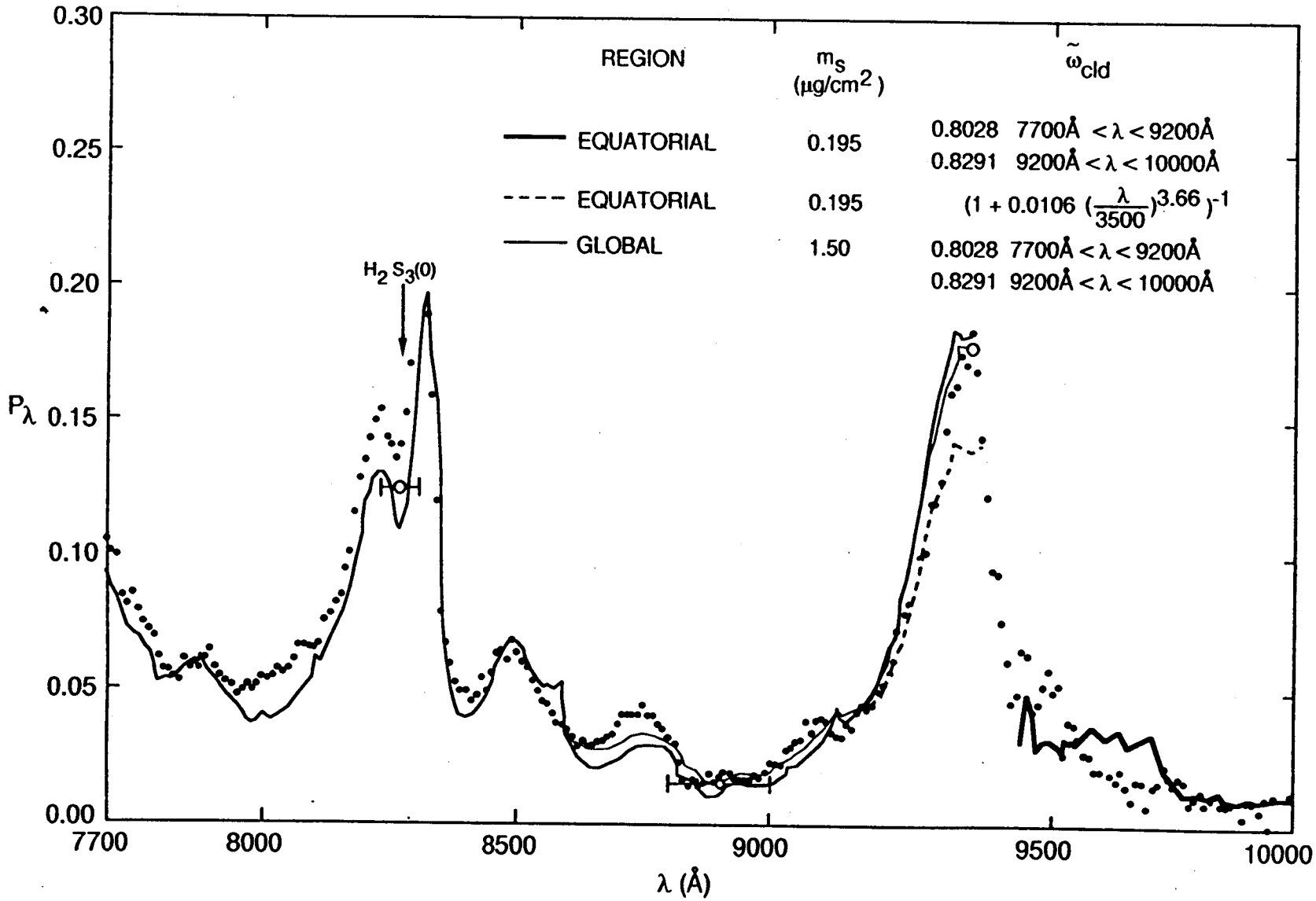
REGION
$m_s$ (μg/cm²)
$\tilde{\omega}_{cld}$
EQUATORIAL 0.195
0.8028 7700Å < λ < 9200Å
0.8291 9200Å < λ < 10000Å
EQUATORIAL 0.195
$(1 + 0.0106\ (\frac{\lambda}{3500})^{3.66})^{-1}$
GLOBAL 1.50
0.8028 7700Å < λ < 9200Å
0.8291 9200Å < λ < 10000Å
$H_2$ $S_3(0)$
$P_\lambda$
0.30
0.25
0.20
0.15
0.10
0.05
0.00
7700
8000
8500
9000
9500
10000
λ (Å)

FIGURE 17

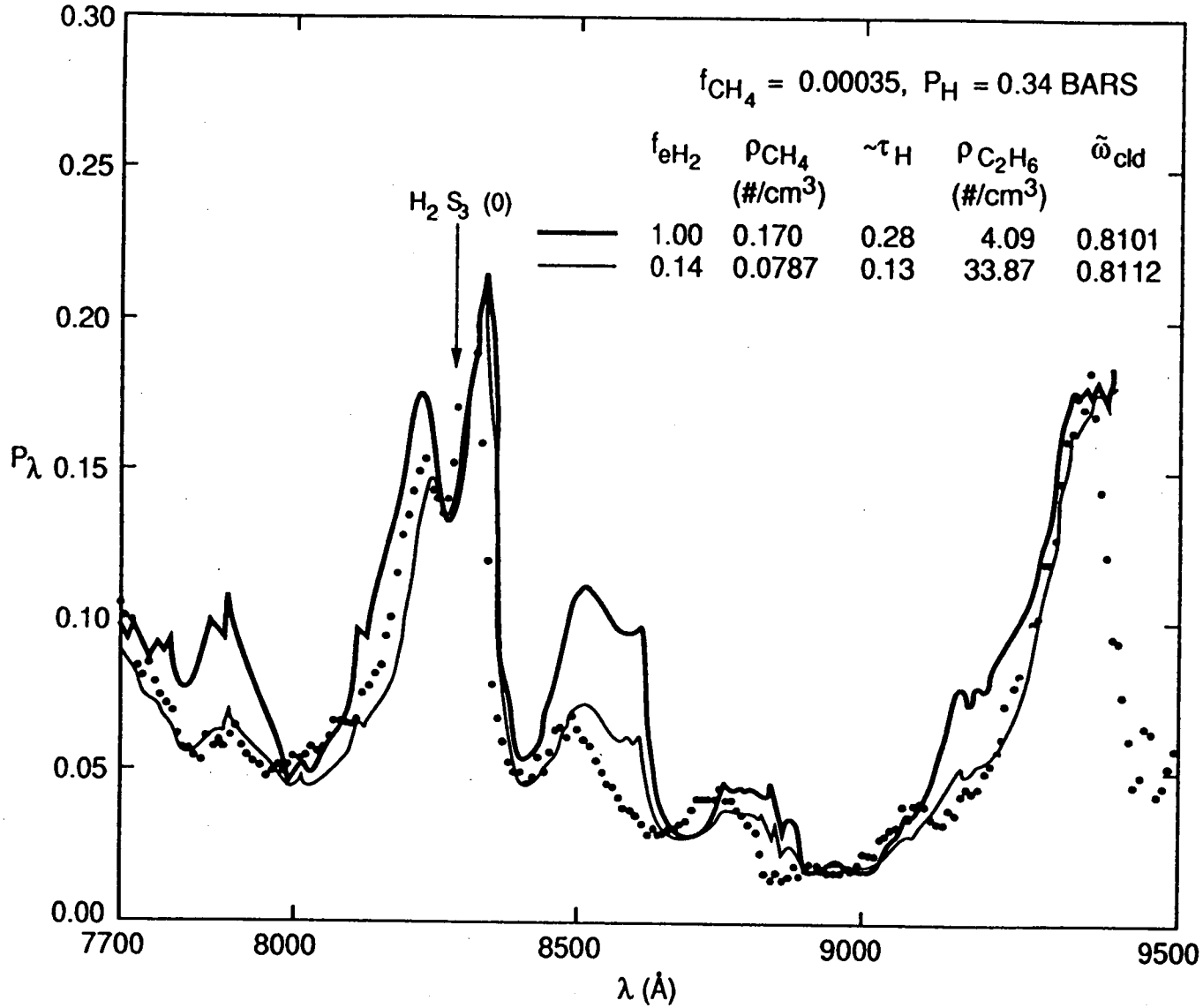
$f_{CH_4}$ = 0.00035, $P_H$ = 0.34 BARS
$f_{eH_2}$ $\rho_{CH_4}$ (#/cm$^3$) $\sim\tau_H$ $\rho_{C_2H_6}$ (#/cm$^3$) $\tilde{\omega}_{cld}$
1.00 0.170 0.28 4.09 0.8101
0.14 0.0787 0.13 33.87 0.8112
$H_2$ $S_3$ (0)
$P_\lambda$
0.30
0.25
0.20
0.15
0.10
0.05
0.00
7700
8000
8500
9000
9500
λ (Å)

FIGURE 18

FIGURE 19

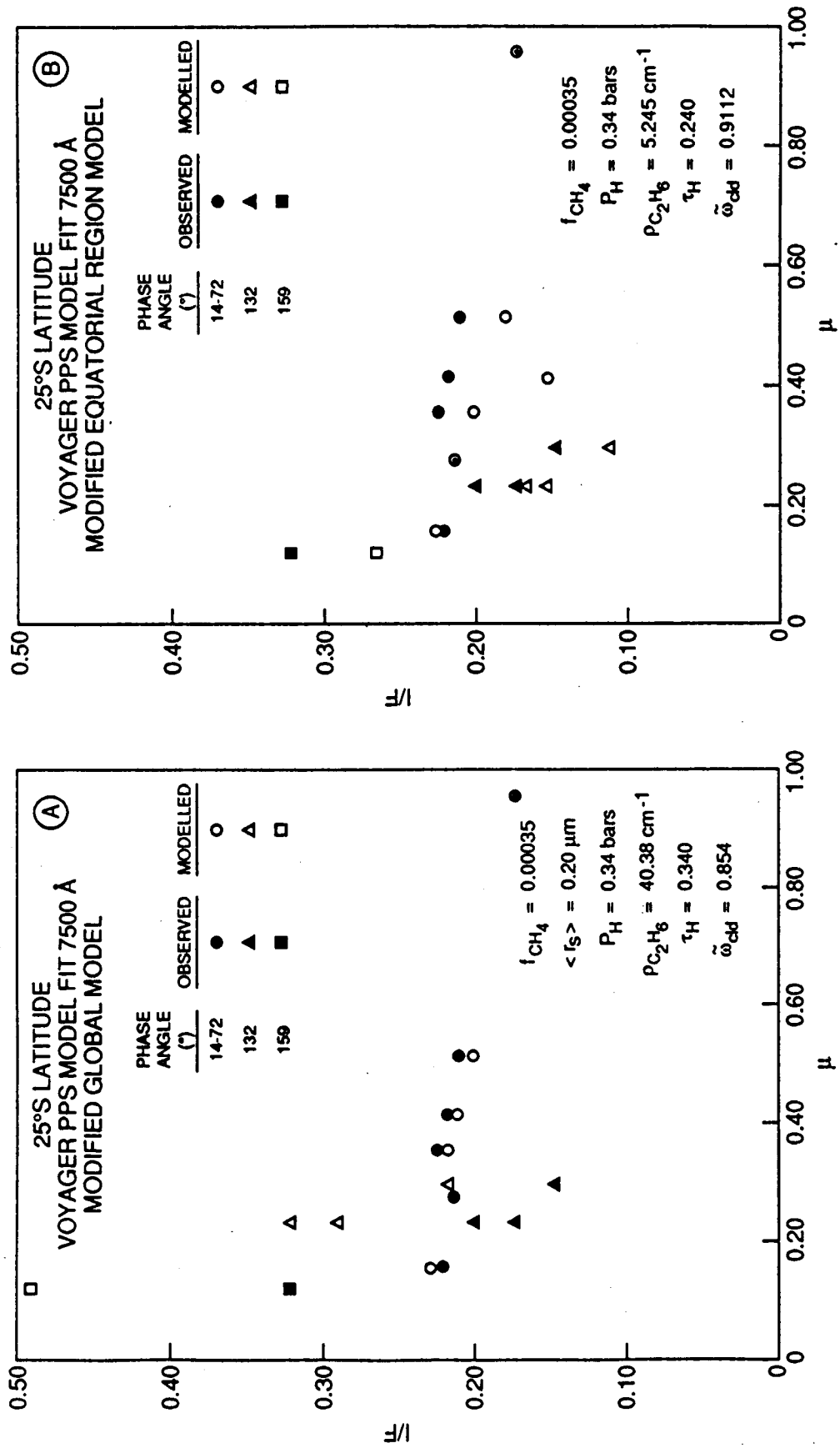
25°S LATITUDE
VOYAGER PPS MODEL FIT 7500 Å
MODIFIED GLOBAL MODEL
(A)
PHASE ANGLE (°)
OBSERVED
MODELLED
14-72
132
159
$f_{CH_4}$ = 0.00035
$\langle r_s \rangle$ = 0.20 μm
$P_H$ = 0.34 bars
$\rho_{C_2H_6}$ = 40.38 cm$^{-1}$
$\tau_H$ = 0.340
$\tilde{\omega}_{cld}$ = 0.854
I/F
μ
25°S LATITUDE
VOYAGER PPS MODEL FIT 7500 Å
MODIFIED EQUATORIAL REGION MODEL
(B)
$f_{CH_4}$ = 0.00035
$P_H$ = 0.34 bars
$\rho_{C_2H_6}$ = 5.245 cm$^{-1}$
$\tau_H$ = 0.240
$\tilde{\omega}_{cld}$ = 0.9112

TABLE I.
NEPTUNE EQUATORIAL REGIONAL STRUCTURE ANALYSIS SUMMARY

| Parameter | Baseline Model (SM2) ($f_{CH_4,s}$ = 0.00035, $P_H$ = 0.34 bars, $\langle r_s \rangle$ = 0.2 μm) | | Overall Constraints (Over all $f_{CH_4}$, s $P_H$, $\langle r_s \rangle$) |
|---|---|---|---|
| | Nominal Value | Uncertainty/Reference | |
| Stratosphere: | | | |
| $f_{CH_4,s}$ | 0.00035 | SM2 definition | $2.5\ 10^{-5}$ - 0.0017 |
| $P_s$ top | 0.0014 bars | Hydrocarbon condensation level | |
| $P_s$ bottom ($C_2H_6$ bottom) | 0.020 bars | | |
| $\langle r_s \rangle$ | 0.200 μm | SM2 definition | 0.1 - 0.25 μm |
| ρ (#/cm$^3$): | | | |
| $C_4H_2$ | 0.059 | -0.044, +0.061 | 0 - 0.18 (for $\langle r_s \rangle$ = 0.2 μm) |
| $C_2H_2$ | 1.057 | -0.786, +1.093 | 0 - 3.23 |
| $C_2H_6$ | 5.245 | -3.900, +5.423 | 0 - 16.54 |
| $N_s$ ($10^6$/cm$^2$) | 8.3 | -6.2, +8.5 | 0 - 26.0 |
| $m_s$ (μg/cm$^2$) | 0.195 | -0.145, +0.200 | 0 - 0.61 |
| $n_i$ (6340) | 0.000 | +0.047 | 0 - 0.05 |
| $n_i$ (7490) | 0.000 | +0.126 | 0 - 0.13 |
| $n_i$ (8260) | 0.000 | +0.149 | 0 - 0.15 |
| $\tilde{\omega}_s$ (6340) | 1.000 | -0.2016 | 0.7 - 1.0 |
| $\tilde{\omega}_s$ (7490) | 1.000 | -0.5 | 0.4 - 1.0 |
| $\tilde{\omega}_s$ (8260) | 1.000 | -0.5 | 0.4 - 1.0 |
| $\tau_s$ (6190) | 0.0245 | -0.0245, +0.0265 | 0 - 0.0747 |
| $\tau_s$ (7270) | 0.0167 | -0.0167, +0.0223 | 0 - 0.0509 |
| $\tau_s$ (8900) | 0.0137 | -0.0137, +0.0173 | 0 - 0.0418 |

NEPTUNE EQUATORIAL REGIONAL STRUCTURE ANALYSIS SUMMARY (CONT)

| Parameter | Baseline Model (SM2) ($f_{CH_4}$s = 0.00035, $P_H$ = 0.34 bars, $< r_s >$ = 0.2 μm) | | Overall Constraints (Over all $f_{CH_4}$, s $P_H$, $< r_s >$) |
|---|---|---|---|
| | Nominal Value | Uncertainty/Reference | |
| Troposphere: | | | |
| $f_{CH_4}$,t | 0.03 | Baines and Smith, 1990 | |
| $P_H$ top | 0.34 bars | SM2 definition | 0.14 – 0.64 |
| $P_H$ bottom | 1.54 bars | Condensation level | |
| Double H – G Model: | | | |
| $g_1$ | 0.900 | Nominal Pryor et al., 1992 | |
| $g_2$ | -0.110 | Nominal Pryor et al., 1992 | -0.22 – -0.07 |
| f | 0.42 | Nominal Pryor et al., 1992 | 0 – 0.7 |
| $\tilde{\omega}_H$ (6340) | 1.000 | -0.13 | ~0.85 – 1.00 |
| $\tilde{\omega}_H$ (7490) | 1.000 | -0.31 | ~0.65 – 1.00 |
| $\tilde{\omega}_H$ (8260) | 1.000 | -0.35 | ~0.60 – 1.00 |
| $\tau_H$ (6190) | 0.085 | -0.018, +0.018 | 0.042 – 0.104* |
| $\tau_H$ (7270) | 0.047 | -0.012, +0.011 | 0.021 – 0.055* |
| $\tau_H$ (8900) | 0.058 | -0.013, +0.011 | 0.026 – 0.065* |
| Mie Scattering Model: $< r_H >$ | 2.50 μm | | |
| $\rho_{CH_4}$ (#/cm$^3$) | 0.053 | ±0.007 | 0.03 – 0.07 |
| $N_H$ ($10^6$/cm$^2$) | 0.16 | ± 0.02 | 0.08 – 2.3 |
| $m_H$ (μg/cm$^2$) | 7.81 | ± 1.09 | 4.0 – 11 |
| $n_i$ (6340) | 0.0 | + 0.0011 | 0 – 0.002 |
| $n_i$ (7490) | 0.0 | + 0.0011 | 0 – 0.002 |
| $n_i$ (8260) | 0.0 | + 0.00017 | 0 – 0.0003 |
| $\tilde{\omega}_H$ (6340) | 1.0 | - 0.0598 | 0.92 – 1.00 |
| $\tilde{\omega}_H$ (7490) | 1.0 | - 0.0524 | 0.92 – 1.00 |
| $\tilde{\omega}_H$ (8260) | 1.0 | - 0.0067 | 0.99 – 1.00 |
| $\tau_H$ (6190) | 0.089 | ± 0.012 | 0.046 – 0.125 |
| $\tau_H$ (7270) | 0.085 | ± 0.012 | 0.044 – 0.120 |
| $\tau_H$ (8900) | 0.086 | ± 0.012 | 0.044 – 0.121 |

NEPTUNE EQUATORIAL REGIONAL STRUCTURE ANALYSIS SUMMARY (CONT)

| Parameter | Baseline Model (SM2) ($f_{CH_4,s}$ = 0.00035, $P_H$ = 0.34 bars, $< r_s >$ = 0.2 μm) | | Overall Constraints (Over all $f_{CH_4}$, s $P_H$, $< r_s >$) |
|---|---|---|---|
| | Nominal Value | Uncertainty/Reference | |
| Bottom Cloud: | | | |
| $P_{cld}$ | 3.3 bars | (Baines and Smith, 1990 nominal) | ± 0.3 bars |
| $\tilde{\omega}_{cld}$ (6340) | 0.915 | ± 0.006 | 0.90 – 0.93 |
| $\tilde{\omega}_{cld}$ (7490) | 0.775 | ± 0.012 | 0.75 – 0.80 |
| $\tilde{\omega}_{cld}$ (8260) | 0.803 | ± 0.010 | 0.78 – 0.82 |

* Giver's (1978) $K_{CH_4}$ increases opacities by 0.01 over those derived here from Karkoschka and Tomasko's (1992) $K_{CH_4}$. Phase function with $g_1$ = -0.900, $g_2$ = -0.21, and f = 0.393, representitive of backscattering limit of Pryor et. al, (1992) decreases opacities by ~0.015

## TABLE II

## STANDARD MODEL PARAMETERS

$\langle r_s \rangle = 0.200\ \mu m$

| MODEL | $f_{CH_4}, s$ | $P_H$ (bars) | $\rho_{C_2H_6}$ | $\tau_H$ | | | $\tilde{\omega}_{cld}$ | | |
|---|---|---|---|---|---|---|---|---|---|
| | | | | 6190 Å | 7270 Å | 8900 Å | 6340 Å | 7490 Å | 8260 Å |
| SM1 | 0.00010 | 0.44 | 4.445 | 0.086 | 0.047 | 0.062 | 0.9117 | 0.7746 | 0.7966 |
| SM2 | 0.00035 | 0.34 | 5.245 | 0.085 | 0.047 | 0.058 | 0.9149 | 0.7753 | 0.8025 |
| SM3 | 0.00100 | 0.14 | 4.445 | 0.084 | 0.046 | 0.059 | 0.9120 | 0.7687 | 0.8000 |

## TABLE III.
## NOMINAL STRATOSPHERIC AEROSOL PROPERTIES AT 0.26 AND 0.75 μm

| REGION | YEAR | ADOPTED MODEL PARAMETERS | | | | DERIVED STRATOSPHERIC HAZE PARAMETERS | | | | | | REFERENCE |
|---|---|---|---|---|---|---|---|---|---|---|---|---|
| | | | Stratospheric Haze | | | | | | | | | |
| | | $f_{CH_4}$ Strat | $C_2H_6$ | | | $<r_s>$ (μm) | Column Mass # Abundance μg/cm² | Column # Abundance $10^6$/cm² | $n_i$ 0.26 μm | $\tau_s$ 0.26 μm | $\tau_s$ 0.75 μm | |
| | | | Top (mbars) | Top (mbars) | Bottom (mbars) | | | | | | | |
| Global Mean | 1981-1986 | 0.03 | 2.0 | 6.0 | 10.0 | 0.52 | 5.7 | 13.1 | 0.004 | 0.42 | 0.45 | Baines & Smith (1990) |
| | | 0.00035 | 1.4 | 10.0 | 20.0 | 0.20 | 1.5 | 63.9 | 0.014 | 0.37 | 0.13 | Baines & Hammel (1993) |
| Equatorial Band | 1986 | 0.025 | 2.0 | NA | 3.0 | I* | NA | NA | 0.6 | NA | 0.12 | Hammel et al. (1989) |
| | | 0.001 | 1.4 | 10.0 | 20.0 | 0.20 | 0.17 | 7.0 | N/A | 0.041 | 0.014 | Baines & Hammel (1993) |
| | | 0.00035 | 1.4 | 10.0 | 20.0 | 0.20 | 0.20 | 8.3 | N/A | 0.048 | 0.017 | |
| | | 0.00010 | 1.4 | 10.0 | 20.0 | 0.20 | 0.17 | 7.0 | N/A | 0.041 | 0.014 | |
| 22°S - 30°S | 1989 | 0.0035 | 5.0 | – | 100.0 | 0.20 | 1.04 | 43 | 0.03 | 0.19 | 0.05 | Pryor et al. (1992) |

I*: Isotropic scattering haze assumed by Hammel et al.(1989). Mie scattering assumed by all other investigations.

## TABLE IV.
## NOMINAL TROPOSPHERIC AEROSOL PROPERTIES AT 0.75 μm

| REGION | YEAR OF DATA | ADOPTED MODEL PARAMETERS | | | | | DERIVED 0.75 - μm AEROSOL PARAMETERS | | | | | REFERENCE |
|---|---|---|---|---|---|---|---|---|---|---|---|---|
| | | $f_{CH_4}$ STRAT | $f_{CH_4}$ TROP | BOTTOM CLOUD TOP (bars) | $CH_4$ – HAZE | | $CH_4$ – HAZE | | | BOTTOM CLOUD | | |
| | | | | | BOTTOM (bars) | TOP (bars) | $\tilde{\omega}$ | $\tau$ | P(θ)* | $\tilde{\omega}$ | P(θ)* | |
| Global Mean | 1981-1986 | 0.03 | 0.03 ** | 3.3 ** | 1.54 | 0.7 | 0.87 | 0.03 | I | 0.94 | I | Baines & Smith (1990) |
| | | 0.00035 | 0.03 | 3.3 | 1.54 | 0.34 | 1.00 | 0.05 | D | 0.80 | D | Baines & Hammel (1993) |
| Equatorial Band | 1986 | 0.025 | 0.025 | 2.6 | 1.5 | 0.40 | 0.6 | <0.05 | I | 0.9985^^ | I | Hammel et al. (1989) |
| | | 0.001 | 0.03 ** | 3.3 ** | 1.54 | 0.14^ | 1.00 | 0.05 | D | 0.769 | D | Baines & Hammel (1993) |
| | | 0.00035 | 0.03 | 3.3 | 1.54 | 0.34^ | 1.00 | 0.05 | D | 0.775 | D | |
| | | 0.00010 | 0.03 | 3.3 | 1.54 | 0.54^ | 1.00 | 0.05 | D | 0.775 | D | |
| 22°S - 30°S | 1989 | 0.0035 | 0.02 | 3.2 | 1.3 | 0.90 | 1.00 | 0.6 | D | 0.7 | D | Pryor et al. (1992) |
| | | 0.0035 | 0.02 | 3.2 | 1.3 | 0.90 | 0.84 | 1.0 | D | 0.84 | D | |
| | | 0.00035 | 0.03 ** | 3.3 ** | 1.54 | 0.34^ | 1.00 | 0.34 | D | 0.854 | D | Baines & Hammel (1993) |

* PHASE-FUNCTIONS DERIVED ONLY BY PRYOR ET AL (1992). OTHERWISE, ARE ASSUMED.

I : ISOTROPIC SCATTERING

D : NOMINAL DOUBLE HENYEY-GREENSTEIN PHASE FUNCTION OF PRYOR ET AL. (1992) : $g_1 = 0.9$, $g_2 = -0.11$, $f_1 = 0.42$

** DEEP-ATMOSPHERE TROPOSPHERIC $CH_4$ MIXING RATIO AND BOTTOM CLOUD TOP PRESSURE, DERIVED IN CONCURRENT MODELING EMPHASIZING $H_2$ AND $CH_4$ LINE PROFILE INFORMATION BY BAINES AND SMITH (1990). DERIVED RANGES: $f_{CH_4} = 0.030 \pm 0.007$, $P_{cld} = 3.2\text{-}3.8$ BARS. $f_{CH_4}$ VARIES WITH $P_{cld}$ TO PRESERVE A $CH_4$ COLUMN ABUNDANCE OF ~ 4.52 km-amagats.

^^ BOTTOM CLOUD OPACITY = 3.0 FOR HAMMEL ET AL. (1989) MODEL. OPTICALLY INFINITE FOR ALL OTHER INVESTIGATIONS.

^ EQUATORIAL REGION $CH_4$ HAZE TOP DERIVED IN BAINES AND HAMMEL (1993) FROM CENTER-TO-LIMB INFORMATION. ACCEPTABLE RANGE IS APPROXIMATELY ± 0.2 BARS ABOUT THE NOMINAL RANGE SHOWN. MAXIMUM ACCEPTABLE: 0.63 BARS.